IMPACT OF ENVELOPE CHOLESTEROL AND SPIKE GP41 ON CELL-INDEPENDENT LYTIC INACTIVATION OF HIV-1 BY PEPTIDE TRIAZOLE THIOLS

A thesis submitted to the Faculty of Drexel University

by

Ramalingam Venkat Kalyana Sundaram

in partial fulfillment of the requirements for the degree

of

Doctor of Philosophy

May 2015

DREXEL UNIVERSITY
School of
Biomedical
Engineering, Science
and Health Systems

DREXEL UNIVERSITY
Graduate School of
Biomedical Sciences
and Professional Studies
College of Medicine

Dedications

- To my mother Savithri and my father Kalyanasundaram, for nurturing my intellectual curiosity and believing this day would come, even when I did not.

- To my sister Devasena, for being a willing companion throughout this journey.

Acknowlegdments

I express my gratitude to Dr. Irwin Chaiken and the late Dr. Elisabeth Papazoglou for accepting me into the PhD program and welcoming me to their individual labs. I thank Dr. Papazoglou for introducing me to Dr. Chaiken, without whom this work would not have happened. I am indebted Dr. Chaiken for his time, his vision, his support and guidance that have helped shape and focus my intellectual curiosity.

Special thanks to my advisory committee comprising of Dr. Adrien Shieh, Dr. Kenneth Barbee, Dr. Fred Allen, Dr. Cameron Abrams and Dr. Steven Wrenn for their time, constructive criticisms and feedback during my PhD. I am especially thankful to Dr. Steven Wrenn who gave helpful insight into membranes and Dr. Cameron Abrams who helped in interpretation and analysis of data.

I am thankful to all my colleagues and friends James Huynh, Karl Weiss, Dr. Rachna Arora, Dr. Adel Ahmad Rashad, Dr. Bibek Parajuli, Dr. Srivats Rajagopal, Dr. Ferit Tuzer, Charles Ang, Lauren Bailey, Andrew Holmes, Caitlin Duffy, Aakansha Nangarlia, Kriti Acharya, Dr. Zulfiya Orynbayeva, Dr. Boris Polyak, Dr. Francesca Santini, Armin Darvish, Dr. Arangaserry Rosemary Bastian, Dr. Ali Emileh, Dr. Chetana Sunkari and John Alamia for guidance, sharing resources and importantly, coffee breaks!

Table of Contents

Table of Figures:

Abstract

Impact of Envelope Cholesterol and Spike gp41 on Cell-Independent Lytic Inactivation of HIV-1 by Peptide Triazole Thiols

Ramalingam Venkat Kalyana Sundaram

HIV-1 is a retrovirus that infects host cells carrying the receptor CD4 and the co-receptor CCR5/CXCR4. The process of infection is carried out by the virus specific proteins gp120 and gp41, expressed as a trimer of dimers on the virus surface. This interaction can be interrupted with the use of peptide triazole thiols (PTT). They are a family of entry inhibitors that carry dual antagonist behavior against gp120 by blocking both CD4 and co-receptor interactions.

The thiol introduced into the PTT sequence by a C-terminal Cysteine adds an additional irreversible inactivating step consisting of lysis leading to the release of capsid p24 protein from the lumen of the virus. Since PTTs do not interact with the membrane as established with viral particles with no spike or particles pseudotyped with VSV-G, lysis must be a consequence of conformational changes within the spike being triggered by PTTs, resulting in membrane perturbation and the eventual mixing of viral luminal contents with the extracellular surroundings. Since there is a similar mixing of viral contents with intracellular contents after CD4/co-receptor interaction with the virus, we decided to use

this lytic event as a window to study the lipid-protein interactions that take place to allow the disruption of the membrane and the eventual release of luminal contents. This study was split into two sections.

In the first section, the lipids that make up the viral lipid bilayer (envelope) were investigated and a thorough survey of literature pointed to cholesterol, the major lipid constituent (*ca.* 45 mol %). Prior literature has shown that depletion with a chemical agent specific for cholesterol, methyl beta-cyclodextrin (MβCD) from the viral envelope or from cells producing viruses resulted in a complete loss of infectivity. When tested for the impact of sterol depletion on lysis with PTT, the results were dramatic. Small amounts of MβCD treatment (< 312 μM) led to a stark increase in the amount of lysis (*ca*. 2.5x base-line lysis) before being suppressed at higher [MβCD]. This correlated with a similar bell-shaped trend in infectivity of HIV-1 pseudotyped spikes but not VSV-G pseudotyped spikes suggesting it was specific to HIV-1.

Further biochemical investigations showed that cholesterol content had mostly dropped (*ca.* 40%) within the small range of MβCD treatment and majority of the spike gp120 had shed, consistent with previous reports on MβCD treatment. The enhancement and suppression of lysis after cholesterol depletion could be reversed by the supplementation of exogenous cholesterol. More crucially, reversal could also be achieved with a sterol that supported rafts (cholestanol) and to a much lesser extent with a sterol that did not (coprostanol). Fluorescent investigations into the viral envelope showed a rise in

membrane fluidity (> 312 μM MβCD) using the probe Laurdan and a bell-shaped quenching of fluorescence using the probe Dehydroergosterol with a nadir in intensity at 312 μM MβCD. These data suggested that the membrane was undergoing morphological changes with the depletion of cholesterol and this was affecting the lysis observed with PTTs and infectivity. The sterol data and DHE data hint at the role of rafts in the transitions observed but this has not been conclusively proven.

To further the understanding, the protein involved with the membrane gp41 was investigated. Different regions of gp41 were examined for their role in lysis through site-directed mutagenesis of the BaL.01 sequence. Of the mutants created, all showed dose-dependent lytic release with PTT treatment in comparable levels and IC_{50}s to the wild-type BaL.01 pseudovirus. While all mutants showed reduced infectivity, which was consistent with literature, mutations at the putative interface between envelope cholesterol and the spike (CRAC -> L676I, C-terminal tail truncation -> R706St) showed enhancement of lysis at [MβCD] lower than that for wild type (~ 10 μM). One possible reason might be that envelope cholesterol that is held tightly by viral spike interactions is more easily removed by MβCD in the mutants.

Mutations that targeted conserved tryptophan residues within the membrane proximal external region (MPER domain) affected the sensitivity to cholesterol depletion, with the mutant containing all Trp residues mutated (W(1-5)A) being the least sensitive. Since these residues are known to be critical for infectivity of HIV-1 and other viruses including

Influenza and Ebola, the data suggest a common purpose for this region in both infectivity and lysis.

Based on the mutational data collected, one may conclude the following: (1) Mutations have a much bigger effect on infectivity than on lysis. (2) Multiple regions of gp41 might be involved in the lytic mechanism, and mutations targeting single regions might not be big enough to stop lysis. (3) Alternatively, none of the regions targeted with mutations are crucial for lysis, though this is very unlikely due to the trends observed with sensitivity to cholesterol.

Taken in context with the cholesterol depletion data, the findings can be explained with an energy to reaction argument. High cholesterol content (~ 45 mol %) results in low fluidity and tight packing of phospholipids, and this might benefit the spike in helping it maintain structure and conformation. However, it raises the energy barrier for the membrane-interacting gp41 protein in processes such as fusion and lysis which require large conformational changes such as the formation of the 6-helix bundle. Removing cholesterol to a limited extent might help lower the barrier, permitting these events to occur at a higher frequency and greater likelihood and this may be why we see an enhancement in lysis and infection.

Investigations into the lytic mechanism with PTTs have provided a potential window into the mechanism of fusion that occurs with HIV-1. This is of critical importance, as there is a pressing need for entry inhibitors and a better understanding of the mechanism might foster a whole new generation of virus-inactivating, lytic entry inhibitors.

Specific Aims

My overall aim was to study the intriguing lipid-protein machinery at the virological synapse that is responsible for the complicated processes of lysis and fusion. I studied this mechanism by splitting off the role of viral lipids (cholesterol) and viral proteins (gp41) in the interplay that leads to lytic release of p24 and correlated any similarities with fusion.

There is an urgent need for entry inhibitors. The market contains effective therapeutics that target the virus after it has entered the host cell. These therapies are focused on keeping the patient alive and leading as normal a life as possible. Entry inhibitors raise the bar on therapeutics by targeting the virus before it enters the cell, transforming the patient of an incurable disease into a healthy individual taking preventatives. Peptide triazoles and peptide triazole thiols represent a class of dual antagonist inhibitors that target a wide range of HIV-1 clades and cause dual antagonism of CD4 and co-receptor binding, shedding of gp120 from the virus spike and for the latter, lytic release of luminal capsid p24 protein. These consequences of PTT treatment make it an attractive therapeutic whose mode of action needs to be studied in greater detail.

The crux of this thesis focused on the aspect of spike triggering by PTT that results in lytic release suggesting that spike protein conformational changes can perturb the surrounding lipid bilayer and possibly disrupt the integrity leading to release of luminal contents into the extracellular milieu. This action mimics an aspect of fusion where the binding of CD4 and co-receptor triggers conformational changes in the spike gp120 and gp41, and eventually results in the fusion of the lipid bilayers of the virus and cell. Hence, using

PTTs as a model allows us to understand how gp41 in concert with the surrounding lipids undergoes membrane perturbation.

The three specific aims for this project included:

Aim 1: Determine the role of cholesterol present in the viral membrane on lytic release of p24 and correlate it with infection.

This aim used a coordinated study between lytic release with KR-13, a PTT and infection on HIV-1 pseudoviruses that are depleted of cholesterol using methyl beta cyclodextrin (MβCD), a chemical that is specific to cholesterol. To determine the impact of depleting cholesterol, assays were run along a same gradient of [MβCD] that determined lytic release with PTT (ELISA for p24), infectivity (chemiluminescence), shedding of spike gp120 (western blots), membrane fluidity (Laurdan fluorescence shift) and membrane morphology with Dehydroergosterol (fluorescence).

Aim 2: Determine and produce mutants within spike gp41 that target its interaction with the lipid bilayer.

This aim focused on prior literature on regions of gp41 known to interact with the membrane and determine mutations that affect these interactions. This was followed by site-directed mutagenesis efforts to create mutant pseudoviruses with different membrane-binding abilities. The produced pseudoviruses were characterized for infection

(chemiluminescence), gp120 content (western blots) and normalized with their p24 content (sandwich ELISA).

Aim 3: Determine the effect the mutations created in Aim 2 have on cholesterol depletion and the difference between these mutants and wild type.

This aim brought together concepts developed in aim 1 after cholesterol depletion and the mutants developed in aim 2 to create a holistic picture on the interplay that takes place between proteins and lipids during lytic release. While a lot of the mutants that target sensitive regions, had little to no infectivity, their lytic behavior will be characterized.

Overall, this work furthered the understanding of lipid-protein interactivity required for concerted processes like lysis and fusion and may enable us to develop classes of entry inhibitors that target this mechanism. It will also enable us to forge new design pathways for PTTs.

Chapter 1: Introduction

PATHOLOGY OF HIV-1

HIV-1 is a virus that infects humans by targeting the cells of the immune system (CD4+ T cells, macrophages and dendritic cells). The disease is thought to spread mainly through the exchange of fluids between two hosts, and in this regard, spread can occur indirectly by the sharing of needles. Estimates (as of 2013) have the number of people who have HIV-1 at 35 million globally with the number of new infections dropping due to the spread of information on safe practices and enhanced access to antiretrovirals that reduce the chance of transmission (UNAIDS Report, 2014).

ENTRY AND LIFE CYCLE OF HIV-1

HIV-1 infects cells through a sequence of steps that start with the interaction of gp120 with the cellular receptors CD4 and CCR5/CXCR4 as shown in **Figure 1**. This is followed by the exposure of the fusogenic tip of gp41, which is believed to become immersed in the lipid bilayer of the host cell. This is followed by the collapse of the heptad repeat region of gp41 (N-HR and C-HR) into a six-helix bundle. Thermodynamic data with peptides that mimic the sequence of this region suggest that the formation of the 6-HB complex

releases enough energy to allow for fusion of the membrane bilayers of the virus and the host cell, allowing the entry of the protein capsid and the genetic material into the cell [1].

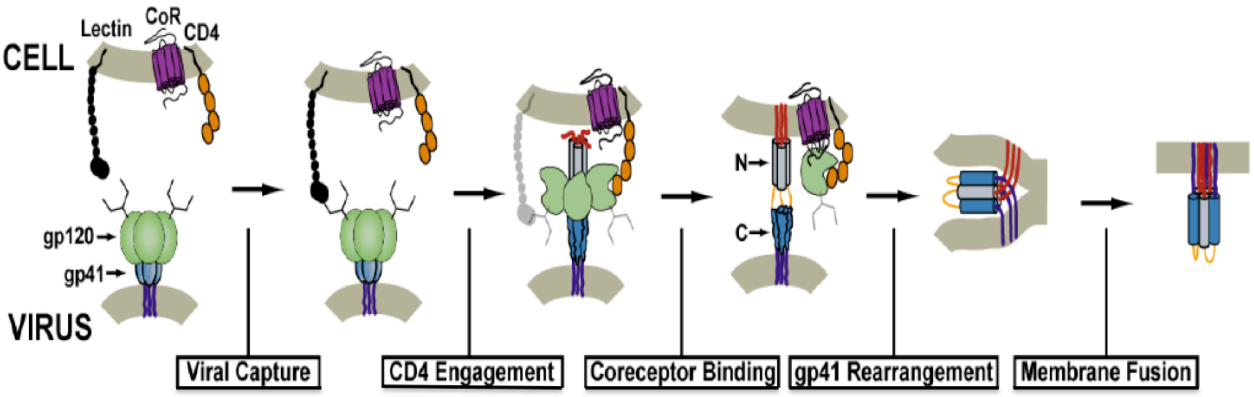

Figure 1: *Depiction of the initial interactions of the viral spike gp120 with host receptors CD4 and co-receptor CCR5/CXCR4 followed by the insertion of the fusion peptide and the formation of the 6-helix bundle that enables fusion. Adapted from [2]*

Once the genetic material has entered the cell, it is acted upon by an enzyme called reverse transcriptase that converts the viral RNA to DNA, which is then shuttled into the nucleus. Here, it is integrated into the host cell genome by another enzyme, integrase, after which the process can stop for a period of time, known as latency or the DNA can be expressed as mRNA immediately to start the translation process of expressing viral proteins. The expressed viral proteins are shuttled from the endoplasmic reticulum, through the golgi and the cell surface where the assembly of viruses begins [3]. The proteins that make up the core of the virus assemble on the inner surface in an immature form, while the spikes

(gp120 + gp41) assemble on the outer surface. Once all the proteins have been assembled, the virus buds off in an immature state. A third enzyme associated with viruses, protease, is responsible for cleaving the immature poly-protein gag (Pr55) into its constituent proteins matrix (MA, p17), capsid (CA, p24), nucleocapsid (NC, p7) and this process is believed to occur immediately after budding [3, 4].

INHIBITORS AGAINST HIV-1 AND THE NEED TO TARGET ENTRY

The steps of the HIV-1 lifecycle have been well studied biochemically and structurally leading to a family of drugs targeting each step known as highly active antiretroviral therapy (HAART). While individual drugs demonstrated great efficacy in *in vitro* studies, they eventually lost activity in human studies due to the heavy rate of mutations the virus undergoes in each generation. The big breakthrough in therapy occurred in 1996 at the International Conference on AIDS, where it was reported that a combination therapy targeting more than one step at a time proved effective at keeping the viral counts low. Recently, the FDA has approved the use of Truvada, a combination of two HAART drugs, Emtricabine and Tenofovir as a pre-exposure prophylaxis. In this case, large human studies have shown that partners of HIV-1 positive individuals (seronegative individuals), taking Truvada were at a much lower risk of contracting HIV-1 compared to people on a placebo. This represented a significant breakthrough in HIV-1 prevention [5, 6]. However, all these steps targeted the virus after it entered the host. There are only two approved drugs that

target the entry step: Fuzeon (Enfuvirtide, Roche), that targeted and inhibited the six-helix bundle formation, and Selzentry (Maraviroc, Pfizer), that targeted the co-receptor, CCR5 and inhibited gp120 from binding to it [7]. Both of these drugs are prone to becoming ineffective due to virus mutations and have to be administered at high levels that often result in unpleasant side effects. This led to their restricted use as salvage therapies after all other drugs had proven to be ineffective. At this stage, there is a pressing need for more effective entry inhibitors.

PEPTIDE TRIAZOLES AND PEPTIDE TRIAZOLE THIOLS

The Chaiken lab has developed peptide triazoles, a sequence of amino acids with an active pharmacophore consisting of Ile-X-Trp where X is a non-natural amino acid, Azidoproline containing a triazole moiety that allows for the facile addition of a bulky metallocene (ethynyl ferrocene) through a copper-catalyzed Click chemistry [8-10]. These peptides target the spike gp120 and inhibit its interaction with both CD4 and co-receptor (CCR5/CXCR4). They also result in the shedding of the spike gp120 from the spike resulting in irreversible inactivation of the virus [11].

A recent generation of this peptide includes a Cys at the C-terminus containing a free thiol and embodies an additional mode of inhibition by causing the lysis of the virus and the

release of capsid protein (p24) from within the viral lumen but with retention of an intact residual particle.

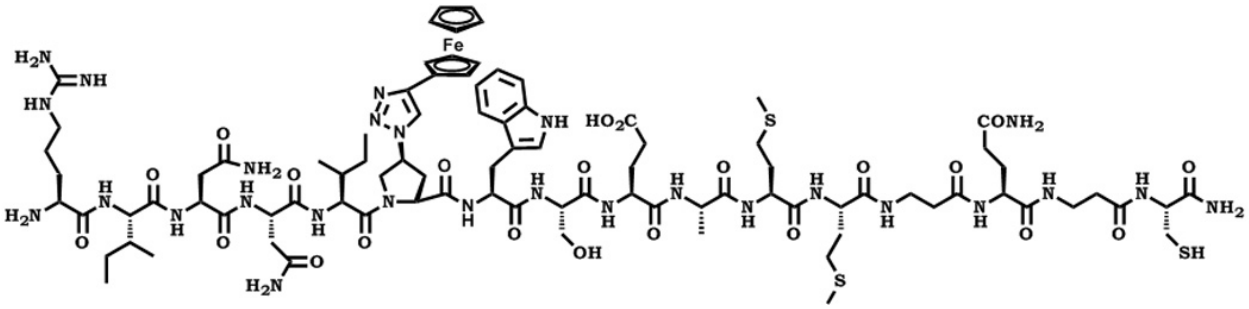

Figure 2: *Sequence of the first generation PTT, KR-13 used in this study. In letter code, the above sequence is: RINNIXWSEAMMBaQBaC where X = Ferrocenyl triazole Pro.*

The lytic activity is specific to viruses carrying HIV-1 gp120 and peptides triazoles carrying a free thiol, since control viruses pseudotyped with VSV-G glycoprotein are not lysed by this peptide, and peptides with the thiol group blocked or the active pharmacophore scrambled do not cause lysis [11]. After a thorough survey of literature, this is the first agent that simultaneously blocks both CD4 and co-receptor from binding to gp120, causes shedding of gp120 from the virus and the release of capsid p24 from the virus lumen without interacting directly with the virus membrane (envelope).

Further investigations have revealed that the process of lytic release by peptide triazole thiols (PTTs) can be inhibited using agents that target and arrest the formation of the 6-helix bundle [11]. Also, treatment with the PTT results in a dose- and time-dependent exposure of the conserved MPER epitope, normally not visible to antibodies [11]. Taking both of these observations together suggests that PTT treatment of HIV-1 results in a sequence of steps including the formation of the 6-helix bundle, which is required for lysis. The requirement to form the 6-helix bundle and expose MPER in the process is similar to the entry steps the virus undertakes for a successful fusion event. These data suggest that PTT-induced lysis involves the manipulation of the viral membrane through concerted conformational changes of the virus spike after the binding of the PTT to spike gp120. To understand the nature of the lipid-protein interaction at the virological synapse that results in lysis, this thesis was focused on the lipids that make up the virus membrane (cholesterol) and the protein that interacts with the envelope (gp41).

THE UNIQUE LIPIDOME OF HIV-1

Lipidomic analysis of HIV-1 virions and the cells in which they are produced argue that virus membranes are mostly made up of cholesterol (45 mol %) [12-14]. This is a common feature amongst enveloped viruses such as Influenza [15, 16], Ebola [17] and Dengue Virus [18]. Cholesterol is crucial for the functionality of the virus, and depleting it from either the virus or the cells that produce the viruses results in viruses with low or no infectivity

[19-23]. The effect of cholesterol depletion on infectivity can be reversed by the addition of exogenous cholesterol [19]. The exact role played by cholesterol has not been decisively defined.

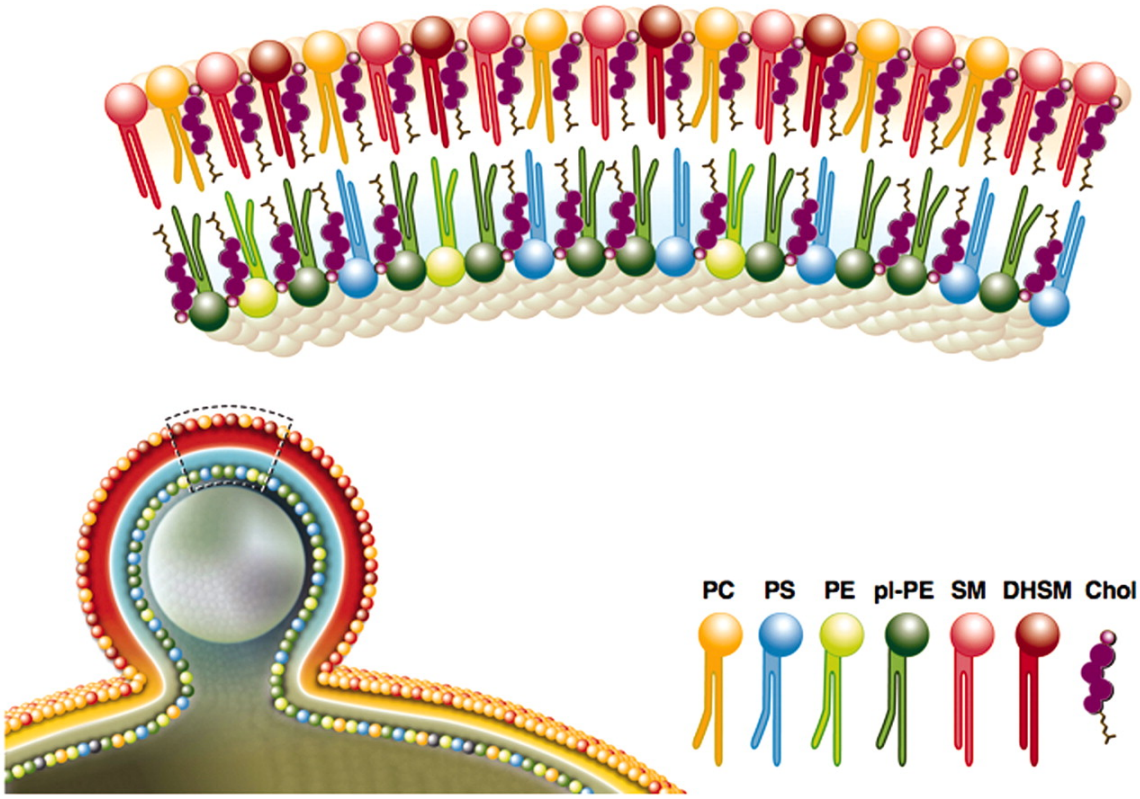

Figure 3: *Distribution of lipids that made up a viral envelope. Adapted from [12]*

Based on evidence with GPCRs including CXCR4, cholesterol is suggested to be a protein structure-supporting lipid [24]. It is packed into membranes at high concentrations so as

to help complex proteins with multiple membrane spanning domains retain structure/conformation as evidenced by the drop in GPCR agonist potency after cholesterol depletion. Others have postulated that lipid bodies like HIV-1 with high radius of curvature due to their small size would be prone to falling apart due to the aqueous exposure of hydrophobic acyl groups of phospholipids. Cholesterol helps as a packing agent, sterically covering hydrophobic regions and enhancing packing [25]. This postulate is supported by the fact that cholesterol content is higher in the outer leaflet than the inner one [12]. Another lipid that is found in high amounts in viral membranes is sphingomyelin (SM) which is exclusively localized in the outer leaflet and is believed to interact with cholesterol through ionic bonds between the hydroxyl group on cholesterol and the amide group in SM [26]. The same group postulated that SM acts as a membrane anchor to hold on to cholesterol in the viral membrane and prevent it from passively falling out [25].

Finally, it has also been shown that lipid rafts are important for HIV-1. HIV-1 buds from the cell membrane raft regions with high local concentration of cholesterol, SM and GM1 based on markers observed on viral membranes that are present in raft regions (CD55) and markers absent on viral membranes, which are not present in raft regions (CD45) [27-29]. Adding to this, Pr55 gag oligomerizes on the inner cell membrane in regions rich in cholesterol [30, 31]. It has also been shown that recovery of infectivity after cholesterol depletion is possible with other sterols that support raft behavior in membranes but not by sterols that do not [19, 20]. These data suggest that sterols of a particular type play an important role in viral infectivity. Hence, a focus of this thesis was to investigate the role

of cholesterol and sterols in general on lysis and compare them with the effect on infectivity.

THE ROLE OF HIV-1 SPIKE PROTEINS IN FUSION

While the lipids that constitute the viral membrane are crucial, regions of the viral spike protein have also been shown to participate in the perturbation of the viral membrane to effect fusion. These regions exist within the transmembrane protein, gp41. This protein can be functionally split into 7 distinct regions starting from the N-terminus: fusion peptide, N-heptad repeat, loop region, C-heptad repeat, MPER domain, transmembrane domain and the cytoplasmic tail. The fusion peptide as mentioned earlier is involved in the interactions with host cells prior to fusion. The N- and C-heptad repeat regions are involved in forming the 6-helix bundle that is believed to bring the cell and viral membranes together. The MPER domain is a region rich in tryptophan residues and the sequence is heavily conserved across all clades of HIV-1 [32, 33]. It is also believed to be involved in fusion based on mutational studies that have substituted the tryptophans to alanines [32, 33].

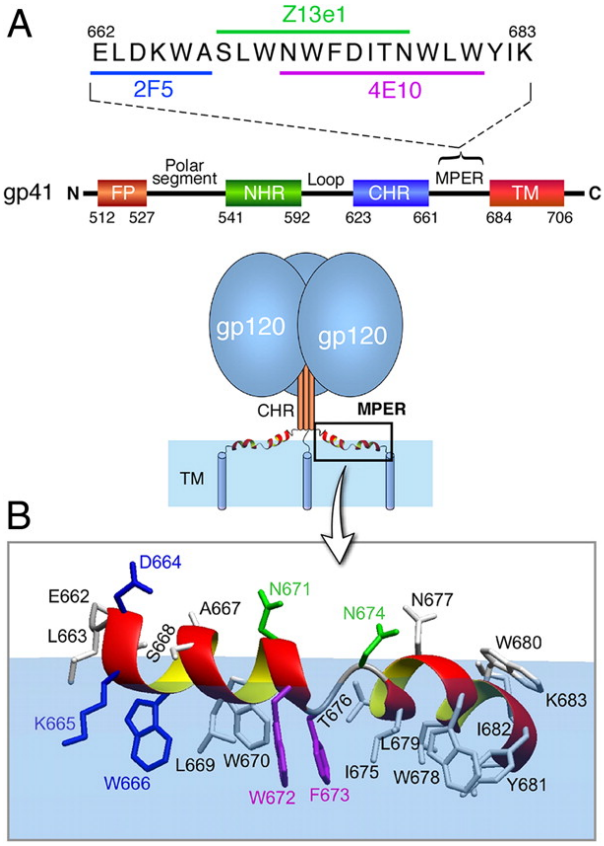

Figure 4: *(A) Sequence and location of MPER in gp41. (B) NMR structure of MPER in lipid micelles illustrating the orientation of conserved Tryptophan residues. Figure adapted from [34]*

The conserved requirement for tryptophans is also seen in other viruses including Influenza and Ebola. The C-terminal residues of this region (LWYIK) form a CRAC domain (Cholesterol Recognizing Amino acid Consensus sequence) and are believed to interact with cholesterol [35-38]. Mutations to the first residue that substitute an Ile for a Leu have a large negative effect on the cholesterol binding ability of the pentapeptide and reduce the infectivity when incorporated into the viral sequence. The transmembrane domain anchors the protein to the viral membrane. It also contains a mid-span arginine, a polar residue in

the middle of a hydrophobic region of the lipid bilayer. This residue is believed to either create a water compartment in the middle of the bilayer or interact with the phospholipid head groups of the inner leaflet, thereby thinning the lipid bilayer [39-41]. This might reduce the energy required to allow for fusion. Finally, the cytoplasmic domain is located at the C-terminus of the protein and, depending upon the clade, can be more than 150 residues long. This region contains three domains known as lentiviral lytic peptides based on the lytic activity these peptides have on lipid bilayers [42]. While little is known about the structure or function of the cytoplasmic tail, they are thought to interact with membrane cholesterol in the inner leaflet [43]. Together, these regions of the virus spike function to manipulate the lipids around them as part of the fusion process.

ESTABLISHING A MODEL TO STUDY THE VIROLOGICAL SYNAPSE

The use of PTTs like KR-13 to effect virolysis suggests that conformational changes in the protein can perturb the surrounding membrane lipids in order to allow the escape of capsid p24. The interactions of viral gp120 with CD4 and co-receptor suggest similarly that spike protein re-arrangement can be used to bring about the formation of a fusion pore and the release of the viral contents into the host cell. The role of protein and lipid interplay is as yet not well understood. The establishment of lysis as a model to study protein mediated lipid perturbation leads to the crux of this thesis.

Chapter 2: Role of Membrane Cholesterol on Lytic Release with PTTs and Infectivity

BACKGROUND:

HIV-1 is an enveloped virus, with a lipid bilayer that separates the contents of the virus from the extracellular milieu. HIV-1 has two surface proteins, exposed on the lipid bilayer, that are used for entry. These proteins, gp120 and gp41, form a trimer of gp120-gp41 heterodimers that is commonly denoted the viral spike or *Env* protein. For productive infection to take place, initial interactions of the viral spike gp120 component with cellular receptors CD4 and CCR5[44] are followed by conformational changes in gp120 that expose gp41 to the host cell membrane. This is followed by the interaction of the fusogenic tip of gp41 with the cell membrane, and rearrangement of the helical heptad repeat regions within each gp41 subunit of the trimer to form a 6-helix bundle, the latter of which brings the viral and cellular membranes into close proximity to allow membrane fusion. Fusion enables the luminal contents including virus genomic RNA, to enter the cell, leading to virus life cycle steps to establish cellular infection. While membrane fusion is known to be critical for virus cell entry and infection, the membrane transformation events occurring during fusion are not fully understood [45].

To inhibit entry of HIV-1, we previously identified peptide triazoles as a class of HIV entry inhibitors that bind to gp120, inhibit it from interacting at either the CD4 or co-receptor binding sites through conformational entrapment [8] and, in the context of the spike, trigger gp120 shedding. KR-13, a peptide triazole thiol (R I N N I **X** W S E A M M βA Q βA C-amide, X = ferrocenyl triazole proline), with a free thiol (PTT) at the C-terminal cysteine residue, not only inhibits HIV-1 infection with nanomolar potency and causes gp120 to be shed from virus, but also triggers release of luminal p24, thus adding, along with shedding, to the irreversible inactivation of virus in a cell-free environment [11, 46]. The release of p24 suggests the ability of the PTT to perturb the viral envelope without directly interacting with the envelope membrane, leading to a loss of membrane integrity. Lytic p24 release appears to not occur through fragmentation of the envelope but rather by more limited membrane transformation, since post-KR-13 treated virions visualized by transmission electron microscopy (TEM) retain an intact though shrunken physical state [11].

In order to identify properties of the envelope that control the lytic inactivation process, we investigated the effect of progressive cholesterol depletion. Cholesterol is a major constituent of the HIV-1 envelope membrane bilayer, making up 45 mol % [12, 14, 47]. Here, we evaluated the effects of cholesterol depletion on KR13-triggered HIV-1 lysis by pre-treating pseudoviruses with methyl beta-cyclodextrin (MβCD). Strikingly, we observed a bell-shaped response of lysis to progressive increase of [MβCD] that included enhancement of function at intermediate [MβCD] even though significant shedding of

gp120, the binding target for KR-13 (PTT), occurred at conditions that induced enhancement of lysis. [MβCD] concentrations enhancing lysis also caused infectivity increase. The enhancement effects on both lysis and infectivity were reversed by adding exogenous raft-promoting sterols. Differential effects of temperature on lysis of untreated *vs* MβCD-treated virus suggested that a decrease in the energy barrier to membrane disruption may be responsible for the parallel enhancement effects of MβCD on lysis and infectivity. Further, the enhancement effects observed here are reminiscent of similar effects reported previously for influenza virus lipid mixing and liposomal fusion [48], as well as HIV-1 infectivity [19], suggesting that cholesterol content provides a balance of function and stability that is found in enveloped virus membranes generally.

METHODS:

GENERAL REAGENTS:

HOS cells expressing CD4/CCR5 were acquired from the NIH AIDS Reagent Program from Dr. Nathaniel Landau. DNA sequences encoding BaL.01 Env and NL4-3 R^- E^- Luc^+ core were also obtained from the NIH AIDS Reagent Program from Dr. John Mascola and Dr. Nathaniel Landau respectively. The plasmid encoding JR-FL gp160 was a kind gift of Dr. Simon Cocklin, while the plasmid encoding YU-2 gp160 was a kind gift of Drs. Alon Herschorn and Joseph Sodroski. Methyl β-Cyclodextrin (MβCD), cholesterol, cholestanol (5α-Cholestan-3β-ol), coprostan-3-ol (5β-Cholestan-3β-ol), dehydroergosterol (Ergosta-5,7,9(11),22-tetraen-3β-ol) and Triton X-100 were purchased from Sigma Aldrich. Laurdan dye was purchased from Invitrogen. Rabbit and mouse anti-p24 and CD45 antibodies were purchased from Abcam. D7324 anti-gp120 antibody was purchased from Aalto.

PROTEIN REAGENTS:

Soluble CD4 (sCD4) was produced and purified as described before [9]. Monoclonal antibody 17b was obtained from Strategic BioSolutions. Wild-type (WT) $gp120_{YU-2}$ was

produced from a pcDNA3.1 vector encoding a V5 (GKPIPNPLLGLDST) coding sequence, N-terminal to the C-terminal HIS_6 tag. The vector also carries the mammalian codon-optimized sequence for a CM5 secretion peptide and $gp120_{YU-2}$ (a gift from Drs. Navid Madani and Joseph Sodroski). DNA for transient transfection was purified using a Qiagen MaxiPrep kit (Qiagen) and transfected into HEK 293F cells according to manufacturer's protocol (Invitrogen). Five days after transfection was initiated, cells were harvested and spun down, and the supernatant was filtered through 0.2 μm filters (Corning). Purification was performed over a 17b antibody-coupled column prepared using NHS-activated Sepharose (GE Healthcare); gp120 was eluted from the column using 0.1M Glycine buffer pH 2.4 into 1M Tris pH 8.0. Identity of the eluted fractions was confirmed by SDS-PAGE and western blotting using antibody D7324 (Aalto Bioreagents). After pooling the peak fractions, additional purification including removal of aggregates was performed with a pre-packed Superdex 200 HR gel filtration chromatography column (GE Healthcare). Monomer-containing fractions were identified by SDS-PAGE/Western blotting with mAb D7324, pooled, concentrated, frozen and stored at -80 °C.

PEPTIDE TRIAZOLE SYNTHESIS AND VALIDATION:

Peptides were synthesized as described before [9, 49] by stepwise solid phase synthesis on a Rink amide resin with a substitution value of 0.25 $mmolg^{-1}$ (Novabiochem). All Fmoc-amino acid derivatives and coupling reagents were purchased from Chem-Impex International Inc. Synthesis-grade solvents were used in all procedures. All peptides were

purified to 98% homogeneity as judged by analytical reversed-phase HPLC on C18. The integrity of purified peptides was confirmed by MALDI-TOF mass spectrometry; observed mass was 2085.43 Da vs. 2085.19 Da expected for KR-13 and 1713.89 Da vs. 1713.33 Da for HNG-156. Peptide triazoles KR-13 and HNG-156 were solubilized in 1x PBS, pH 7.2 and their absorbances measured at 280 nm with a quartz cuvette in a Shimadzu UV1700 spectrophotometer. The concentrations were determined using extinction coefficients of 5965 $M^{-1}cm^{-1}$ and 6090 $M^{-1}cm^{-1}$ for HNG-156 and KR-13, respectively. The functionality of peptides was tested by CD4 and 17b competition assays using surface plasmon resonance (SPR) analysis with a Biacore 3000 optical biosensor.

PSEUDOVIRUS PRODUCTION:

Pseudoviruses were produced as described before [9, 50]. Briefly, HEK 293T cells (3 x 10^6) were co-transfected with 4 μg of BaL.01 gp160 plasmid and 8 μg of NL4-3 $R^- E^-$ Luc^+ core DNA, using Polyethyleneimine (PEI) as a transfection vehicle. YU2 and JR-FL pseudoviruses were produced in an identical manner as BaL.01 pseudoviruses. After 72 hours, the supernatant containing virus was collected and filtered using a 0.45 μm filter (Corning) before being purified via gradient centrifugation on a 6% - 20% Iodixanol gradient (Optiprep, Sigma Aldrich) spun in an Sw41 Ti rotor (Beckman Coulter) at 110, 000 x g for 2 hours at 4 °C. The bottom 5 mls were collected and diluted in serum free medium before being aliquoted and frozen at -80 °C. Importantly, viruses isolated by the

Iodixanol gradient method were found to contain no exosomes as judged by the absence of CD45 (Figure S1). The diagnostic presence of CD45 in exosomes but not viruses has been reported before [51] . All batches of pseudovirus were titrated for infectivity and p24 content immediately after production.

TREATMENTS OF VIRUS WITH MβCD AND PEPTIDE TRIAZOLES:

All MβCD treatments were performed with freshly solubilized powder in PBS. Treatments involved mixing virus samples with MβCD (1:1, v/v) and incubating for 30 minutes at 37 °C. For lysis experiments, the samples were immediately treated with PTT or controls except for the temperature-dependence experiment. For the latter experiment, samples were first treated with 78 μM MβCD or PBS for 30 minutes at 37 °C and then moved to incubators at different temperatures (4 °C, 8 °C, 16 °C, 23 °C, 30 °C, 37 °C and 42 °C) and equilibrated for 15 minutes. Simultaneously, solutions containing PTT were added to separate tubes and also equilibrated at the appropriate temperatures. At the 15 minute time point, all solutions were mixed and incubated for another 30 minutes. All samples were then spun and tested for leaked p24 capsid protein. The amount of lysis was divided by 1800 seconds to produce a "pseudo-rate of lysis (k)" whose natural log was then plotted against the inverse of the absolute temperature (1/T) at which lysis occurred. The slopes were calculated from best-fit lines determined using the linear fitting algorithm provided by Origin Pro 9.0.

For shedding experiments, pseudovirus samples were spun immediately after 30 minutes of MβCD treatment for 2 hours at 21,130 x g. For infectivity experiments, samples were washed to remove MβCD by Iodixanol gradient centrifugation. For infectivity experiments involving cholesterol reconstitution, samples were treated with MβCD for 30 minutes at 37 °C, washed, treated with exogenous cholesterol for another 30 minutes at 37 °C and then fractionated by centrifugation in a gradient composed of Iodixanol (Optiprep, Sigma) (6% - 20%) diluted in PBS. After running the 2 hour spin at 110,000 x g at 4 °C, fractions were collected and tested for p24 content and infectivity.

A competition ELISA between KR-13 and either CD4 or 17b binding for gp120 was used to rule out any effect of MβCD on KR-13 function. For this assay, 96 well high binding ELISA plates were coated with 100 ng/well of soluble gp120 protein overnight (16 hours) at 4 °C. Following a blocking step with 3% BSA in PBS, samples of CD4 (final 30 nM) or 17b (co-receptor surrogate, final 15 nM) were mixed (1:1 v/v) with KR-13 in 0.5% BSA with/without MβCD and loaded onto the plate. The plate was incubated at room temperature for 2 hours with agitation before being stained, for CD4 by Anti-human CD4 biotinylated OKT4 (eBioscience) and then Streptavidin-HRP, and for 17b by secondary antibody anti-human IgG conjugated to HRP. This was followed by a 30-minute incubation with ortho-phenylenediamine (OPD) dissolved at 0.4 mg/ml in sodium citrate with perborate to measure colorimetrically the bound CD4 and 17b using absorbance on a Tecan Infinite m50 plate reader at 450 nm. Each plate contained positive (CD4 or 17b only) and negative (no protein) controls that provided a window for the signal.

PROTEASE TREATMENT OF HIV-1 PSEUDOVIRUSES:

HIV-1 pseudovirus supernatants collected from transfections were concentrated to 500 µL/sample. Samples were labeled as "control" or "protease". Both samples received 500 U of EndoH enzyme (New England Biolabs) diluted in 10 µL of G5 buffer. Samples were flicked to promote mixing and then incubated at 37 °C for 60 minutes. For the protease sample, 1 µg/ml of each of Proteinase K, Chymotrypsin (SigmaAldrich) and Trypsin (Cellgro) were added and flicked to promote mixing as per the protocol developed by Crooks et al [52]. For the control sample, a matching volume of PBS was added and the samples were incubated for 60 minutes at 37 °C. One tablet of protease inhibitors (Complete Mini, Roche, Germany) was dissolved in 10 mls of 1X PBS. 500 µl of the inhibitor mix was added to each tube after 60 minutes of protease treatment. Both samples were then purified on an Iodixanol gradient as described for the pseudovirus production above.

P24 RELEASE DETECTION BY SANDWICH ELISA:

p24 sandwich ELISAs were performed as described before [11]. Briefly, 96 well high binding ELISA plates (Corning) were coated with 50 ng/well of mouse anti-p24 and incubated on a rocker overnight (16 hours) at 4 °C. The antibody solution was mixed before being blocked with 3% BSA in PBS, pH 7.2 for two hours at room temperature on

a rocker. The plate was washed briefly with PBS containing 0.1% Tween – 20 (PBS-T) before being loaded with samples.

Virus stocks were diluted in PBS, pH 7.2, so as to contain 50 ng/ml p24 content in the final sample to be loaded on the plate. The diluted virus was mixed with MβCD in PBS (1:1 v/v) through inversions and incubated at 37 °C for 30 minutes. KR-13 or HNG-56 (non-lytic peptide) or PBS (negative control) was then added to all the tubes (1:1, v/v), and the samples were all mixed by inversions before incubating for another 30 minutes at 37 °C. The 1.5 ml tubes were then spun for 2 hours at 4 °C at 21,130 x g. The top 100 µl of supernatant was carefully removed so as not to disturb the pelleted virus debris. This supernatant was then diluted (1:1, v/v) in PBS containing 1% BSA and 1% Triton X-100. A p24 standard (Abcam, 50 ng/ml) was used in every assay in the same buffer. 50 µl/well of sample was then loaded onto the prepared ELISA plates. The plate was incubated at 4 °C overnight (16 hours) on a rocker before being washed 3 times with PBS-T. The plate was then stained with rabbit anti-p24 primary antibody, followed by donkey anti-rabbit HRP conjugate (GE Biosciences) as a secondary antibody. Both were incubated for 1 hour at room temperature sequentially in PBS containing 0.5% BSA with steady agitation. The plate was washed before the addition of OPD. Plates were developed for 30 minutes in the dark and the absorbance measured at 450 nm to determine endpoint values using an Infinite m50 (Tecan) plate reader.

PSEUDOVIRUS CELL INFECTION ASSAY:

Pseudoviral infection assays carried out as described previously [9, 50] were used to validate the viruses used in this work and to track the effects of MβCD on infectivity. Briefly, HOS.T4.R5 cells were seeded the day before at 7000 cells, 100 µl/well in 96 well plates. Virus stocks were diluted in growth media such that the final dilution gave 1 x 10^6 luminescence counts. Cells were seeded the day before at 7000 cells, 100 µl/well in 96 well plates. When used, MβCD was mixed with diluted virus (1:1, v/v) through inversions and incubated at 37 °C for 30 minutes. Controls were mixed with an equivalent amount of PBS and no MβCD. The samples were then washed using 6-20% Iodixanol gradient. Medium was removed from the plates and virus-containing medium was added. The plates were incubated for 24 hours at 37 °C before the medium was changed. 48 hours after the virus was added to the plate, the medium was removed and the cells were lysed (Passive Lysis Buffer, Promega). The lysate was then transferred to a white well plate (Greiner) and mixed with 1 mM Luciferin salt (Anaspec) diluted in 0.1 M potassium phosphate buffer containing 0.1 M magnesium sulfate and the luminescence measured using a Wallac 1450 Microbeta Luminescence reader at 490 nm.

ENZYMATIC QUANTIFICATION OF PSEUDOVIRUS CHOLESTEROL:

Cholesterol was quantified using a previously established enzymatic method [53]. Samples of pseudovirus treated with different amounts of MβCD were rinsed thoroughly with 1x PBS prior to quantification using the enzymes Cholesterol Oxidase and Horse Radish Peroxidase. The efficiency of MβCD removal sufficed, based on tests with MβCD alone resulting in background signal. Samples of virus were mixed with Cholesterol Oxidase (1 U/ml), Horse Radish Peroxidase (1 U/ml) and Amplex Red (150 μM, 10-acetyl-3, 7-dihydroxyphenoxazine) in PBS and incubated in the dark in a white well plate (Greiner) for 30 minutes at 37 °C before being read in a fluorescence plate reader (Synergy 4, Biotek, Ex/Em (nm): 560/590).

VIRUS GP120 SHEDDING QUANTIFICATION USING WESTERN BLOTS:

gp120 shedding induced by MβCD alone (no PT present) was measured using Western blots as described before [11]. Briefly, MβCD was mixed with virus stocks (1:1, v/v) and incubated at 37 °C for 30 minutes before being spun for 2 hours at 21,130 x g at 4 °C. Sample supernatants were mixed 1:1 with Laemmli buffer and boiled at 95 °C for 5 minutes before being loaded onto 10% SDS-PAGE gels. After gel electrophoresis, the protein was transferred onto a 0.45 μm PVDF membrane (Immobilon-P, Millipore), blocked with 5% milk solubilized in PBS containing 0.1% Tween-20 and then stained with sheep anti-gp120

(D7324, Aalto) followed by Donkey anti-sheep HRP (Invitrogen) antibodies. Luminol substrate (Advansta) was added and the protein bands exposed on chemiluminescence film (Blue Ultra, Genemate) and developed (M35-A X-OMAT Processor, Kodak). The developed film was then scanned and the corresponding image analyzed with Image J (NIH) densitometry.

VIRUS GP41 QUANTIFICATION USING ELISA:

Samples of pseudovirus were treated with the full range of MβCD and incubated at 37 °C for 30 minutes before being spun for 2 hours at 4 °C at 21,130 x g. The supernatant was removed and the remaining pellet was mixed thoroughly by pipetting before being fixed. Samples were fixed in a solution containing 1% Paraformaldehyde and 0.1% Glutaraldehyde at 4 °C for 15 minutes before the fixative was quenched using 0.1 M Glycine. The fixed virus samples were adsorbed overnight (16 hours) on an ELISA plate on a rocker at 4 °C. gp41 protein (NIH AIDS Repository) was also adsorbed on the same plate. The plate was blocked with 200 µl/well of 3% BSA in PBS for 2 hours before being stained sequentially with gp41 antibody 50-69 followed by anti-human HRP (Millipore) and OPD development. All values were normalized to the untreated virus control as 100% and a PBS blank as 0%.

STEROL RECONSTITUTION ASSAY:

Sterol reconstitution was performed using cholesterol, coprostanol or cholestanol. Powder samples were solubilized in chloroform and then diluted in 1x PBS (1:19 v/v) to make up 10 mM stocks in glass vials. Samples were vortexed thoroughly to create a milky emulsion immediately prior to use. Virus samples were pre-treated with MβCD prior to the addition of the sterol. The sterol was incubated with the pseudovirus for another 30 minutes at 37 °C prior to the addition of KR-13 and a subsequent third incubation step for 30 minutes at 37 °C. The samples were then pelleted by centrifugation at 21,130 x g for 2 hours and the supernatant tested for p24 capsid protein via p24 sandwich ELISA. An intact virus sample (treated with only PBS) and lysed virus sample (treated with 1% Triton X-100 before pelleting through centrifugation) formed the 0% and 100% window. Additional controls included MβCD + KR-13 and individual MβCD and sterol treatments to confirm that there was no non-specific lytic release of p24.

Samples used in the infectivity assay were prepared in the same way as above, except that they were rinsed with serum free medium 3x for 3 minutes each at 2000 x g in Amicon concentrators (100 kDa MWCO, Millipore) before being aliquoted in 1.5 ml centrifuge tubes. Cholesterol was serially diluted in PBS and then added to each tube. Samples were incubated for 30 minutes at 37 °C before being run through a 6 to 30 % Iodixanol gradient. Fractions from the gradient were added to HOS.T4.R5 cells in a 96-well plate. The rest of the protocol was carried out as a regular infectivity assay as mentioned above.

For samples treated with only 5000 μM MβCD prior to sterol treatment, a stock of virus was treated with 5000 μM MβCD for 30 minutes at 37 °C before being added to 1.5 ml centrifuge tubes. Solutions of exogenous cholesterol, coprostanol or cholestanol were serially diluted from 5000 μM before being mixed with the MβCD-treated samples of pseudovirus. The tubes were inverted to mix the sterol with the virus before being incubated at 37 °C for another 30 minutes. Samples were then incubated with KR-13 or PBS (negative control) for a final 30 minutes before being spun for 2 hours. Then samples were treated as above to complete a p24 ELISA.

PSEUDOVIRUS VISUALIZATION USING TEM:

Virus samples were treated with MβCD for 30 minutes at 37 °C before being washed thrice at 2000 x g for 3 minutes each in Amicon concentrators (100kDa MWCO). Samples were fixed in solution containing 1% Paraformaldehyde and 0.1% Glutaraldehyde at 4 °C for 15 minutes. Samples were washed again before being mixed with 1% osmium tetroxide and incubated with gentle shaking at 4 °C for 1 hour. Samples were washed seven times with deionized water before being concentrated to 100 μl volume and loaded on Lacey carbon grids (EM Microscopy) and dried overnight. Just before imaging, samples were stained with 0.1 % uranyl acetate and rinsed. Imaging was performed on a JEOL 2100 transmission electron microscope at 120 keV.

MEMBRANE FLUIDITY ANALYSIS:

Membrane fluidity was probed using the fluorescent dye Laurdan (6-dodecanoyl-2-dimethylaminonaphthalene) according to the protocol of Lorizate et al [53]. Briefly, Laurdan was mixed with virus (final concentration 1 μM) for 30 minutes at 37 °C before being washed using a 100 kDa Amicon Ultra concentrator 3 times at 2000 x g for 2 minutes. Samples of virus were then mixed with different concentrations of MβCD for 30 minutes at 37 °C before being imaged on a plate reader (Biotek, Synergy 4) (Ex/Em: 400nm/440nm (blue), 490nm (red)). Fluidity was calculated in Generalized Polarization (GP) units, where GP > 0 denotes ordered domains, while GP < 0 denotes disordered membranes. The formula used was:

$$\text{Generalized Polarization (GP)} = \frac{(I_B - I_R)}{(I_B + I_R)}$$

where I_B = Intensity at 440 nm, and I_R = Intensity at 490 nm

FLUORESCENT STEROL REPORTER ANALYSIS OF MEMBRANE STATE:

HIV-1 pseudoviruses were stained with the fluorescent dye 7-dehydroergosterol (DHE, SigmaAldrich) that has a preference [54-57] for liquid ordered (raft) phase of membranes. DHE was dissolved in chloroform to make a stock solution. Immediately prior to each experiment, the concentration of the dye was measured in methanol using UV-Vis absorbance. Pseudoviruses were stained with 0.5 μM (final concentration) dehydroergosterol for 30 minutes in the dark at room temperature with constant agitation. Following this, excess dye was removed by running the virus + dye mixture through a PD-10 desalting column (GE) before being treated with MβCD for 30 minutes at 37 °C in the dark. All fluorescence measurements were performed in the presence of 1 M potassium iodide as a collisional quencher to ensure only membrane bound dye remained fluorescent. The measurements were performed using the Synergy 4 (Biotek) plate reader monochromator (Ex/Em, nm: DHE 330/425). Untreated virus was used as 100% control, while a PBS sample was used as a 0% control.

MATHEMATICAL ANALYSIS:

All the data presented as percentages in this paper were subjected to a linear interpolation equation, for which controls in each individual experiment defined the 0% and 100% signal windows, and for which linearity within the signal window was established.

RESULTS:

EFFECT OF MβCD PRE-TREATMENT ON THE LYTIC INACTIVATION OF HIV-1 BY THE PEPTIDE TRIAZOLE THIOL KR-13

We investigated the role of membrane cholesterol in KR-13 (PTT) triggered HIV-1 perturbation and p24 release by measuring the effect of virus pre-treatment with increasing concentrations of MβCD. Pseudotyped HIV-1 viruses were first treated with a range of [MβCD] for 30 minutes, followed by addition of KR-13 or a non-lytic parental peptide triazole, HNG-156 (R I N N I **X** W S E A M M-amide, X = ferrocenyl triazole proline).

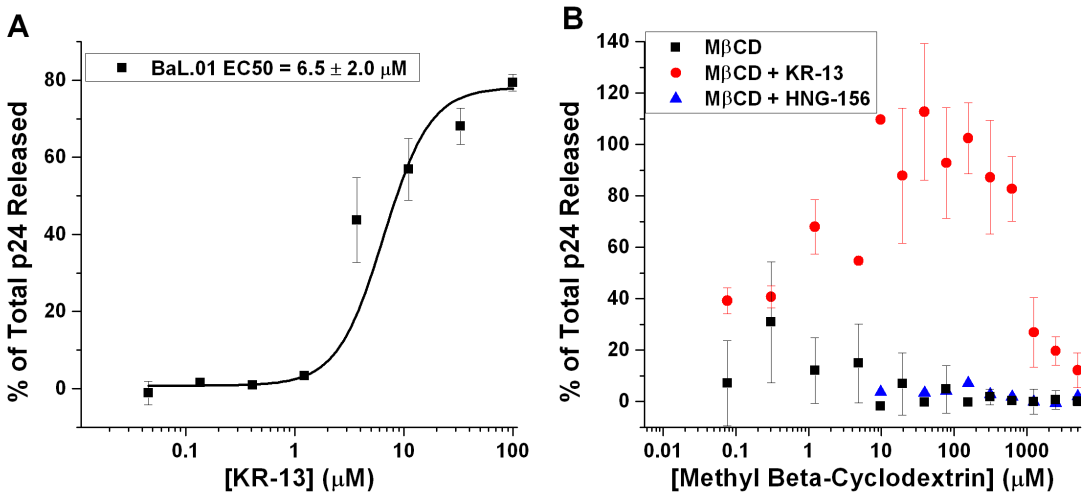

Figure 5: *Lytic release of p24 from HIV-1 pseudovirions after treatment with MβCD and PTs. Contents of p24 were measured by sandwich ELISA. (A) KR-13 dose-dependent release of p24 from BaL.01 pseudoviruses. (B) p24 release as a function of MβCD treatment. Samples of virus were treated with MβCD followed with PBS (black squares), non-lytic parental peptide HNG-156 (blue triangles) or the lytic peptide, KR-13 (red circles), (n=5, mean ± SD).*

The concentrations of KR-13 used were based on the EC_{50} value first determined for p24 release (**Figure 5**A); this value was similar to that observed before [11]. The concentration of HNG-156 used was 5 μM (final). Treated samples were centrifuged to separate the pelleted virus fraction from the released p24 in the soluble protein fraction. The latter was assayed by sandwich ELISA for p24 content. When pre-treated with MβCD, the KR-13 treated samples (red circles, **Figure 5**B) showed an initial marked increase in p24 release up to a maximum between 10 and 312 μM MβCD followed by a steep decline at higher concentrations. No p24 release was observed with the addition of either PBS alone (black squares, **Figure 5**B) or HNG-156 (blue triangles, **Figure 5**B), indicating that the enhancement observed with MβCD was specific for KR-13.

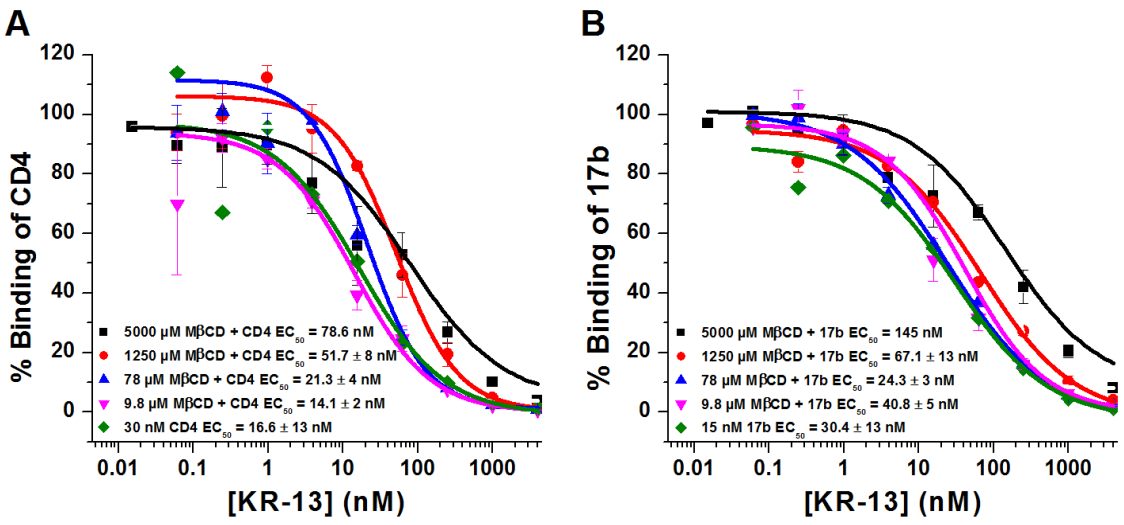

Figure 6: *Competition profiles of KR-13 with CD4 (A) and mAb 17b (B) for binding to gp120 in the presence of MβCD at 5000 μM (black squares), 1250 μM (red circles), 78 μM (blue triangles), 9.77 μM (pink triangles) and 0 μM of MβCD (green diamonds) (n=3, average + SD).*

Control experiments (**Figure 6**) showed that MβCD had no direct effect on KR-13 binding to soluble gp120. Since MβCD at high concentrations (> 10,000 μM) has been reported previously to cause lysis [21], we evaluated the effect of MβCD alone and found that doses below 10,000 μM did not cause p24 release (**Figure 5**B).

BOTH CHOLESTEROL DEPLETION AND GP120 SHEDDING OCCURRED AT MβCD CONCENTRATIONS THAT CAUSED ENHANCED LYSIS

Cholesterol loss induced by MβCD has been measured previously using a fluorimetric assay [58-60]. We used this assay to compare the effect of MβCD treatment on cholesterol content with effects on p24 release and infectivity. Samples of MβCD-treated virus were washed with 1x PBS and then mixed with a cocktail containing cholesterol oxidase, horseradish peroxidase and 10-acetyl-3,7-dihydrophenoxazine (Amplex Red) to provide a fluorescence readout corresponding to cholesterol content. Treatment with 1x PBS alone was used as a negative control, while untreated pseudovirus was used to determine the 100% value for cholesterol content.

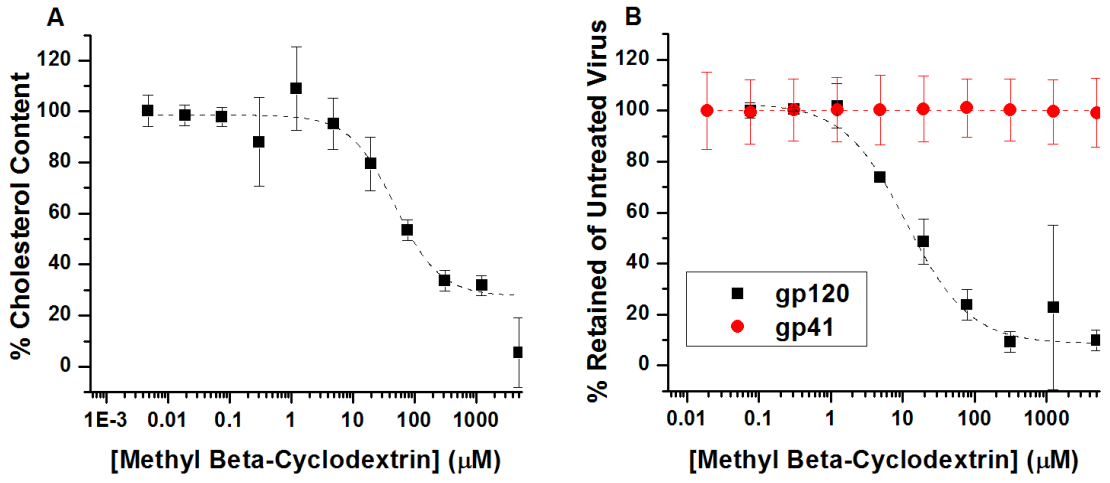

Figure 7: *Biochemical changes of BaL.01 pseudoviruses caused by MβCD treatment. (A) Change in HIV-1 envelope cholesterol content normalized to untreated envelope following MβCD treatment using the fluorimetric readout from the*

Amplex Red assay (n=2, mean ± SD). (B) Quantification of HIV-1 spike proteins that are retained after MβCD treatment. gp120 (black squares) was assayed from the supernatant and retained gp41 (red circles) was assayed from the pellet fraction (gp120: n=2, gp41: n=4, mean ± SD).

The results, shown in **Figure 7**A, confirm a dose-dependent depletion of envelope cholesterol content upon MβCD treatment, with a mid-point at ~50 μM. Of note, the envelope cholesterol depletion was incomplete at the highest [MβCD] used. Since cholesterol depletion was found (data not shown) to be greater (by 30% at intermediate MβCD concentrations) after addition of sphingomyelinase, which converts envelope sphingomyelin to ceramide [61], it is possible that the incomplete removal of cholesterol by MβCD could be due at least in part to stabilizing sphingomyelin-cholesterol interactions in the HIV-1 membrane [62].

We also examined whether the known effect of MβCD on gp120 shedding [21-23] occurred at the concentrations found to affect lysis. Pseudovirus-associated gp120 and gp41 were examined, using Western blots and ELISA, respectively (Methods). The data obtained (**Figure 7**B) show that gp120 was released from the residual virus in a dose-dependent manner, with a mid-point at ~10 μM, while gp41 was retained in the virus fraction.

Since gp120 shedding analysis showed that a large amount of the spike associated gp120 had shed at MβCD concentrations for which KR-13-induced lysis activity was high, we considered it likely that inactive (misfolded) spikes were being selectively shed. The

presence of inactive spikes was confirmed by treating pseudoviruses with Endo H and proteolysis with trypsin, chymotrypsin and proteinase K, as used previously to selectively remove aberrant Env spikes [52, 63]. Enzyme-treated virus samples were purified on an Iodixanol gradient before being characterized for infectivity in chemiluminescence assays, gp120 quantitation with Western blots, and p24 content using sandwich ELISA for virus quantitation. Resulting pseudovirus samples were used in p24 release and gp120 shedding assays. While the gp120 content decreased markedly (~50%) with enzyme treatment (data not shown), infectivity of the viruses was not affected (data not shown), as was also found previously [52]. Importantly, as shown in **Figure 8**A, enzyme treated viruses exhibited a bell-shaped response to [MβCD] for lysis by KR-13 similar to that observed (**Figure 5**B) with viruses not treated with enzymes.

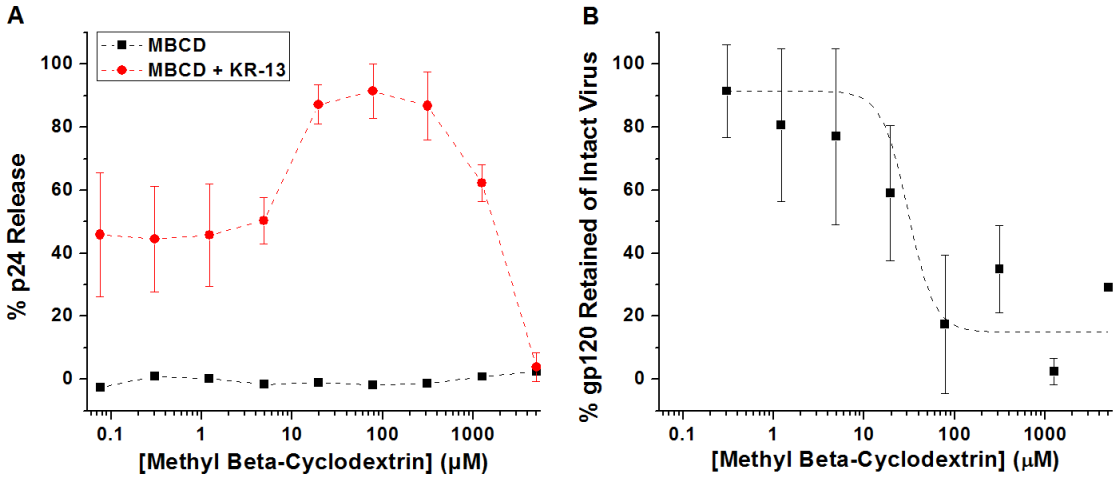

Figure 8: *Sensitivity of p24 release and gp120 shedding of enzyme-treated BaL.01 HIV-1. (A) p24 release from pseudoviruses treated with MβCD alone (black squares) and MβCD with KR-13 (red circles). (B) Virus gp120 shedding in response to MβCD treatment. (n=2, average + SD).*

REVERSIBILITY OF MβCD-INDUCED EFFECTS BY STEROL REPLENISHMENT

We evaluated the extent to which the enhancement effects of cholesterol depletion on lytic inactivation could be reversed by the addition of exogenous cholesterol. HIV-1 pseudoviruses were first treated with MβCD, then with exogenous cholesterol and finally with KR-13. Each treatment was for 30 minutes at 37 °C. Samples were spun to pellet virus, and the supernatants were tested for p24 content. PBS treatment was substituted for both MβCD and cholesterol treatments as a negative control (**Figure 9**).

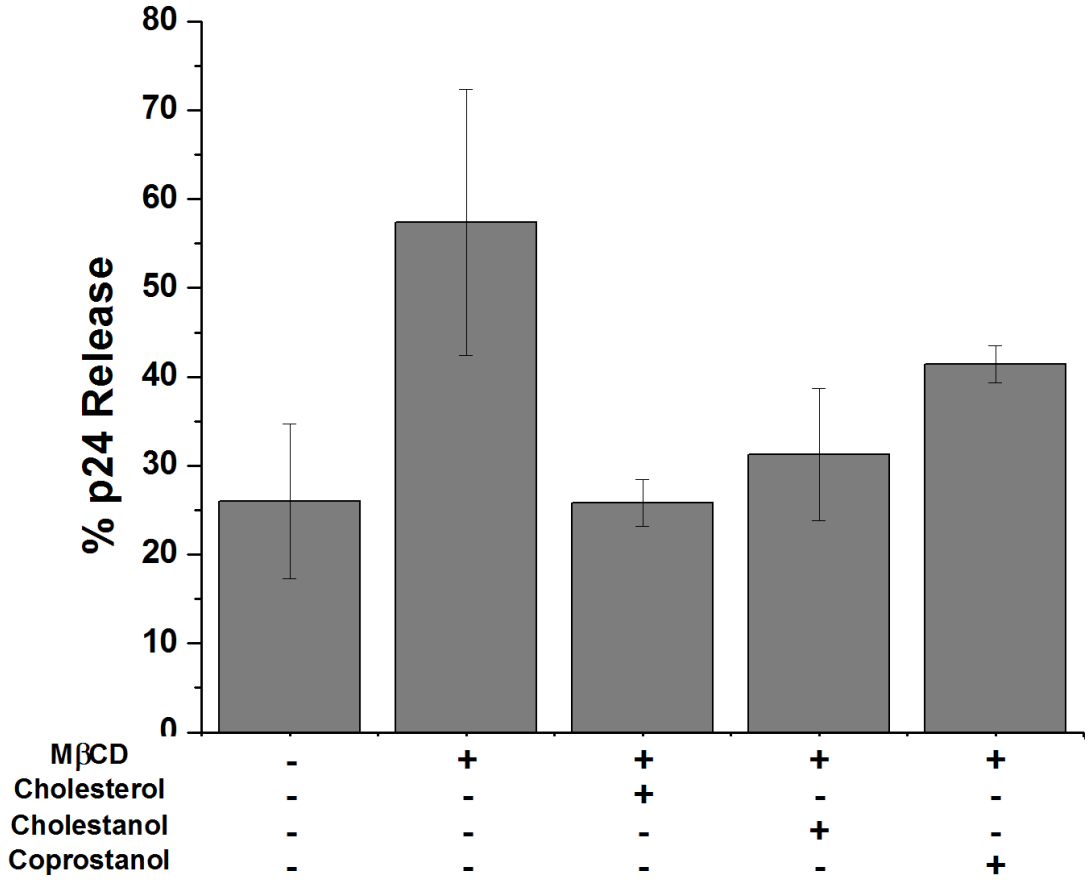

Figure 9: *Lysis properties of BaL.01 pseudoviruses treated with MβCD and then reconstituted with exogenous sterol before the addition of KR-13. Samples were first treated with PBS (-), 78 μM MβCD (+) or 5000 μM MβCD (+++) before the addition of 78 μM cholesterol, cholestanol or coprostanol. All samples were then treated with the KR-13 (at 5 μM) to determine p24 release (n=3, mean ± SD).*

For virus samples in which cholesterol depletion resulted in an enhancement of p24 release (specifically 28% to 57% at 78 μM MβCD), the addition of exogenous cholesterol reduced the observed enhancement. Conversely, in virus samples for which cholesterol depletion led to a suppression of lysis (28% to 5% at 5000 μM MβCD), addition of exogenous

cholesterol led to a partial recovery. The full set of cholesterol replenishment results obtained are reported in **Figure 10**.

We evaluated the extent to which sterol derivatives with different capacities to support membrane raft formation and consequent HIV-1 infectivity [19] would support KR-13-induced p24 release by evaluating viruses reconstituted with cholestanol and coprostanol instead of cholesterol.

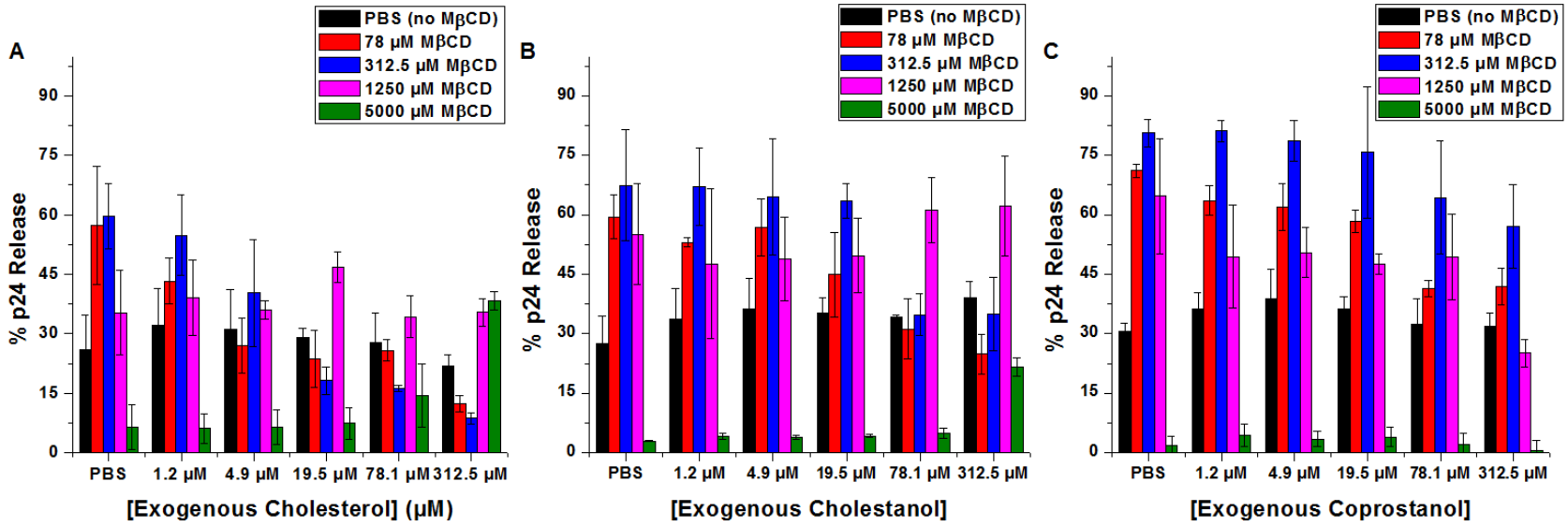
A
B
C
PBS (no MβCD)
78 μM MβCD
312.5 μM MβCD
1250 μM MβCD
5000 μM MβCD
% p24 Release
0
15
30
45
60
75
90
PBS
1.2 μM
4.9 μM
19.5 μM
78.1 μM
312.5 μM
[Exogenous Cholesterol] (μM)
[Exogenous Cholestanol]
[Exogenous Coprostanol]

Figure 10: *Reversibility of cholesterol depletion from pseudoviral membranes. Bar graphs show p24 release from KR-13-treated HIV-1 pseudoviruses after reconstituting with cholesterol (A), cholestanol (B) and coprostanol (C) by sandwich ELISA. Pseudoviruses were treated with PBS (black), 78 μM MβCD (red), 312.5 μM MβCD (blue), 1250 μM MβCD (pink) or 5000 μM MβCD (green) before sterol reconstitution was performed. (n=3, mean ± SD).*

Pseudovirus treated with PBS throughout the experiment was used as the intact virus control (0%), while a detergent-treated sample of pseudovirus was used as the lysed control (100%). No lysis was observed to occur with any of the sterol variants in the absence of KR-13 (data not shown). As shown in **Figure 9**, exogenous cholestanol reversed the effect of cholesterol depletion, though the cholestanol-enabled recovery was reduced compared to that with cholesterol. In contrast, coprostanol induced a much lower suppression of lysis at 78 μM MβCD and no recovery at 5000 μM MβCD. The reduced effect of coprostanol is most evident in **Figure 10**C and the sample of virus treated with 5000 μM MβCD and then with increasing amounts of sterol (**Figure 11**, black triangles).

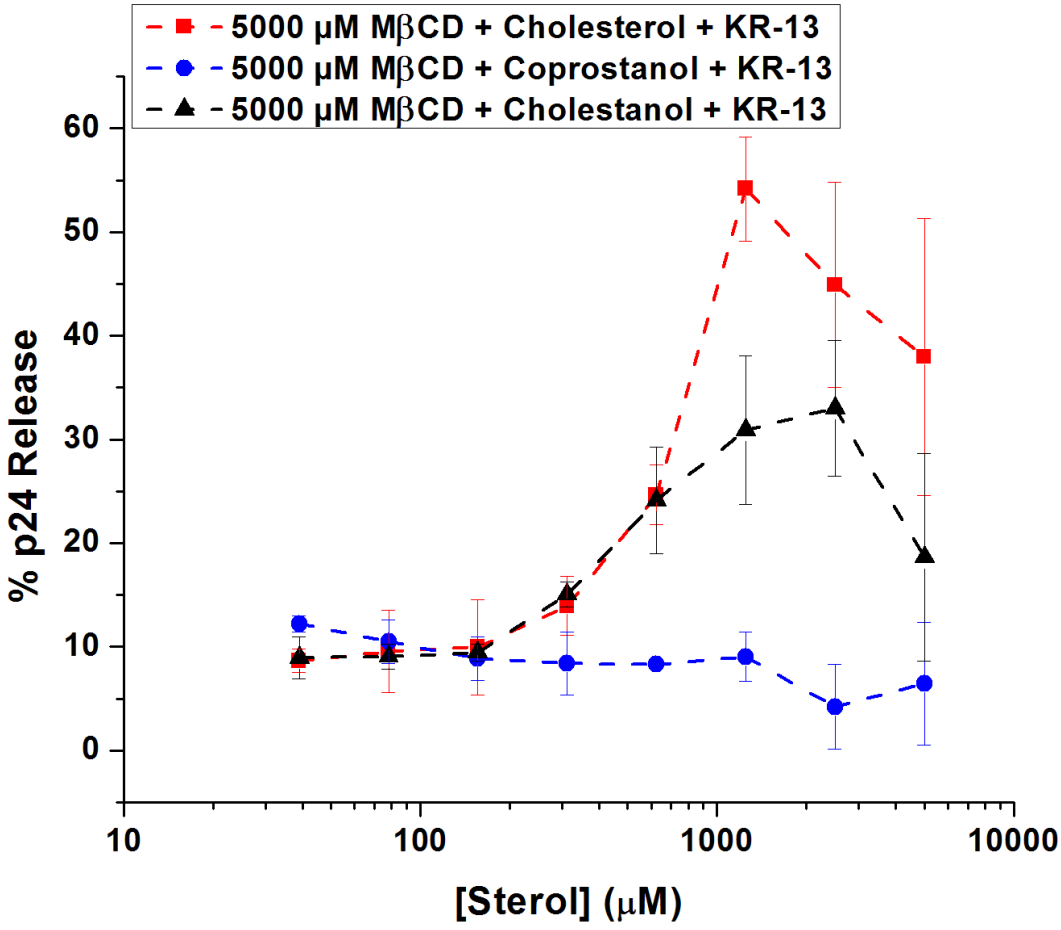

Figure 11: *Raft-supporting sterol requirement for reversibility of MβCD depletion of cholesterol. Samples of BaL.01 pseudovirus were first treated with 5000 μM MβCD for 30 minutes at 37 C followed by replenishment with cholesterol (red squares), coprostanol (blue circles), or cholestanol (black triangles) for another 30 minutes and finally KR-13 before being spun to separate the released protein from virus debris. The released protein was detected by sandwich ELISA. (n=3, mean ± SD)*

Importantly, the above results show that the effectiveness of a sterol to reverse cholesterol depletion effects on KR13-induced lysis parallels its ability to support raft formation in HIV-1. The functional importance of cholesterol rafts in virus infection has been previously reported [19].

EFFECTS OF MβCD ON THE PHYSICAL PROPERTIES OF HIV-1 PSEUDOVIRUS MEMBRANE AT CONDITIONS OF LYSIS ENHANCEMENT AND SUPPRESSION

We evaluated the morphological and biophysical transitions resulting from MβCD treatments affecting KR-13 induced lytic inactivation. Untreated and 5000 μM MβCD treated pseudoviruses were fixed and imaged on a JEOL 2100 transmission electron microscope. Images of untreated and MβCD-treated pseudovirions (**Figure 12**A and B) were not significantly different in size (117.5 ± 34.7 nm vs. 123.1 ± 41.8 nm respectively, n=30, mean ± SD). This observation, along with the finding of gp41 retention after lysis (**Figure 7**B), supports the conclusion that the virion remains intact after MβCD treatment in the absence of KR-13 exposure.

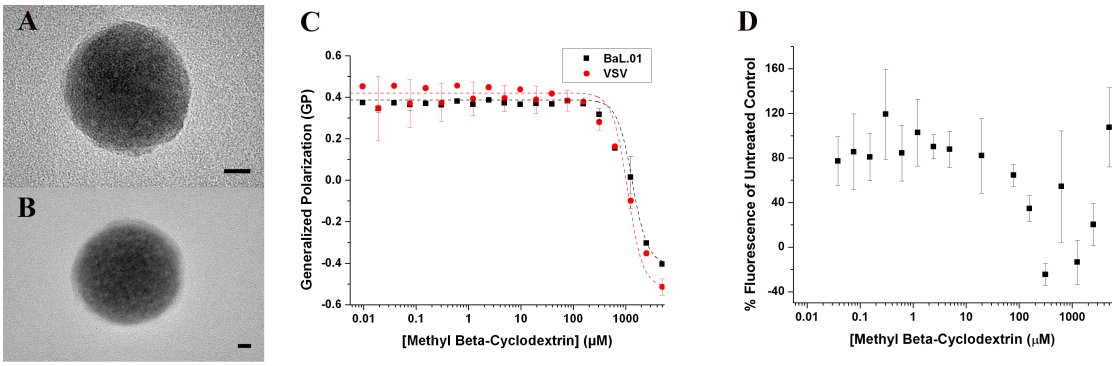

Figure 12: *Physical effects of MβCD on pseudoviruses. (A and B) TEM micrographs of untreated (diameter: 117.5 ± 34.7 nm, mean ± SD, n=30) (A) and 5000 μM MβCD treated (diameter: 123.1 ± 41.8 nm, mean ± SD, n = 30) (B) pseudoviruses. Scale bars represent 20 nm. (C) Change in fluidity of the lipid envelope of HIV-1 (BaL.01, black squares) and VSV-G (red circles) pseudotyped viruses (n=3, mean ± SD) as detected by Laurdan fluorescence. (D) Changes in bulk membrane fluorescence of BaL.01 pseudoviruses first loaded with DHE and then treated with a range of MβCD concentrations in the presence of 1 M potassium iodide (n=5, mean ± SD)*

It has been shown previously using electron spin resonance (ESR) [64, 65] and fluorescence [53] that cholesterol depletion can result in more fluid membranes, and this was confirmed on both BaL.01 and VSV-G pseudotyped viruses using Laurdan in the current study (**Figure 12**C). Importantly, however, a major shift in fluidity was observed only at high [MβCD] (> 312 μM), with no change at lower [MβCD] where increase in lysis was complete (**Figure 5**B).

We evaluated changes in membrane sterol environment by a previously-developed fluorescence assay using dehydroergosterol (DHE) [66], a sterol that preferentially localizes in raft-like regions [54-57]. When treated with MβCD, DHE fluorescence emission was incrementally quenched at [MβCD] > 10 μM, with a fluorescence minimum at ~312 μM MβCD, after which emission recovered (**Figure 12**D). The experiment was performed in the presence of 1M potassium iodide, which should quench any DHE extracted from the membrane by MβCD. Hence, the fluorescence measured is taken to reflect membrane incorporated DHE only. Importantly, the "inverted bell-shaped" curve of DHE fluorescence suggests that a membrane transformation occurred at the same [MβCD] as the enhancement of lysis.

MβCD PRE-TREATMENT REDUCES THE ACTIVATION ENERGY FOR LYSIS

We asked whether cholesterol depletion might lower the energy barrier to KR13-induced membrane lysis. Lytic inactivation by KR13 has been found previously [11] to require gp41 6-helix bundle formation, a transformation that likely involves traversing an energy barrier. A lower energy barrier for KR13-induced lysis could explain why greater lytic release occurred at increasing [MβCD] even though the content of gp120, the binding target for KR13, was decreased. Samples containing equal amount of pseudovirus were treated with PBS (control) or 78 μM MβCD for 30 minutes at 37 °C before being transferred to an incubator at different temperatures (4, 8, 16, 23, 30, 37 and 42 °C). Temperature-equilibrated PBS containing KR13 was mixed, and the samples incubated for another 30 minutes. All samples were then spun and the p24 contents of the fractions containing released protein were measured using sandwich ELISA.

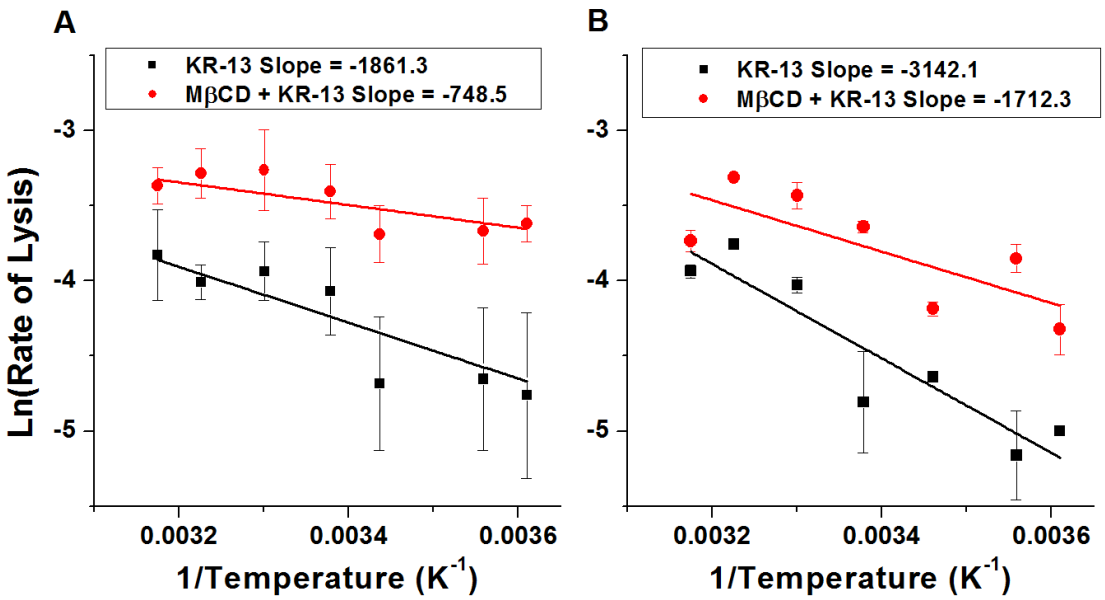

Figure 13: *Comparison of temperature dependence of virus lysis with and without MβCD pretreatment. Samples were treated with 78 μM MβCD (red circles) or PBS (black squares) for 30 minutes at 37 °C followed by an equilibration time of 15 minutes at different temperatures ranging from 4 °C to 42 °C. Samples were then mixed with temperature equilibrated PTT (A: 5 μM KR-13, B: 2 μM KR-13) in PBS and incubated for another 30 minutes before being spun to separate released p24 protein from virus pellets. Released p24 was measured by sandwich ELISA. (n=3, mean ± SD)*

As shown in **Figure 13**A, the slope of the lysis activity increase as a function temperature decreased for the MβCD-treated virus, suggesting that the activation energy for lysis was greater without MβCD pre-treatment. Similar data were obtained in experiments with less KR13 (2 μM, **Figure 13**B), showing that the differences in temperature response are consistently observed at different extents of lytic reaction. These data are consistent with the hypothesis that the activation energy for lysis is reduced after MβCD pre-treatment.

CORRELATION OF EFFECTS OF CHOLESTEROL DEPLETION ON KR13-INDUCED LYSIS AND VIRUS INFECTIVITY

The enhancement of HIV-1 lytic inactivation by MβCD treatment observed in the current work is similar to prior findings of enhanced HIV-1 infectivity by MβCD [19]. This correlation suggests a common effect of cholesterol depletion on the virus membrane transformation events occurring in virus membrane lysis induced by peptide triazole thiols and virus-cell membrane fusion occurring during infection. We sought to confirm the finding of infectivity enhancement with viruses used in the current lysis study. Samples of BaL.01 HIV-1 pseudotyped viruses were treated with PBS (control) or 78 μM MβCD before being washed and added to cells expressing receptors. HIV-1 BaL.01 pseudovirus infectivity indeed was enhanced a [MβCD] conditions that cause lysis enhancement (**Figure 14**).

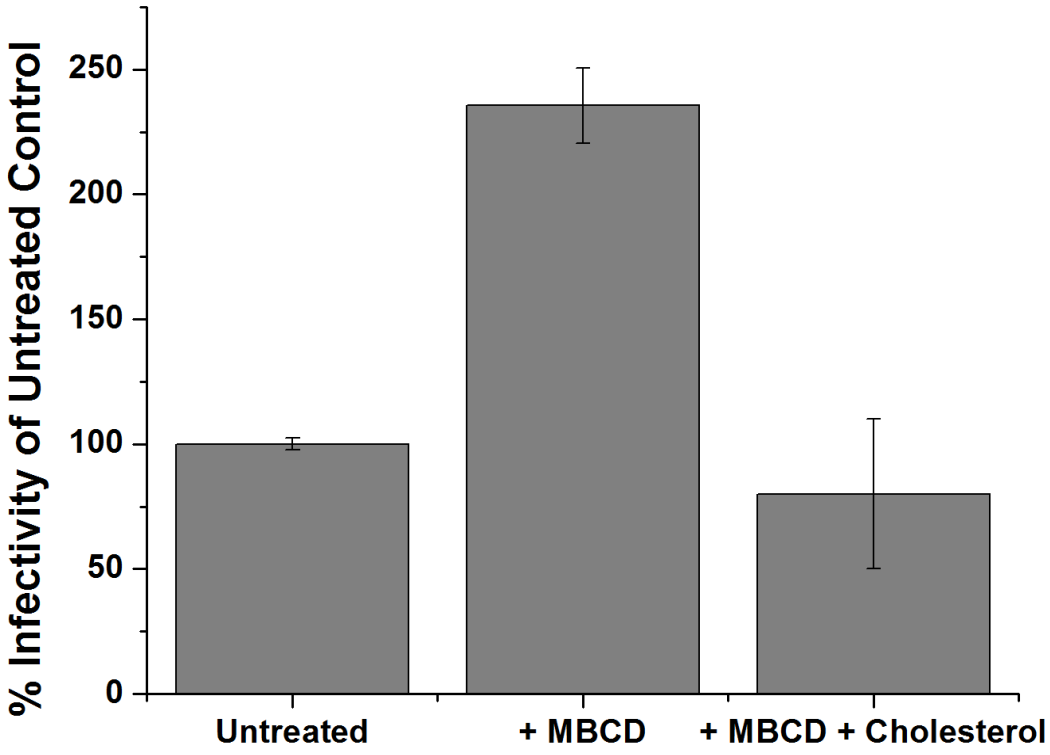

Figure 14: *Infectivity of BaL.01 pseudoviruses treated with PBS, 78 μM MβCD and 78 μM MβCD followed by 78 μM of exogenous cholesterol (n=2, mean ± SD)*

When a similar treatment was performed on viruses without pseudotyped spikes (containing the capsid core coated with a lipid bilayer), neither lysis nor infection was observed in the [MβCD] dose range examined (data not shown). When the MβCD treatment was performed on virus-free cells, which were then washed before addition of untreated viruses, no change in infectivity was observed (data not shown). Of note, infectivity enhancement was also observed in the current work with JR-FL and YU2 (a tier 2, less easily neutralized strain vs. a lab adapted strain) pseudotyped HIV-1 (142% vs 210 % respectively,

Figure 15C). The variable extent of infectivity enhancement observed with these latter viruses fits with the prior finding of more subdued MβCD enhancement effects reported with other pseudotyped viruses (LAI, 150% [19]).

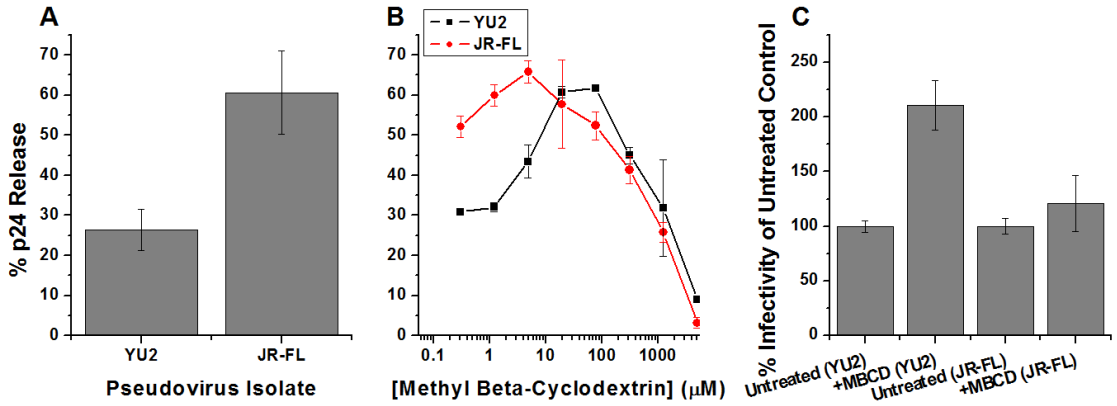

Figure 15: *Comparison of MβCD pre-treatment effects on lysis and infectivity on other HIV-1 isolates. (A) Amount of lysis observed with 5 μM KR-13 (PTT) for YU2 and JR-FL pseudoviruses; (B) Amount of lysis observed for YU2 and JR-FL pseudoviruses with MβCD pre-treatment before the addition of PTT; (C) Change in infectivity with MβCD treatment for YU2 and JR-FL pseudoviruses (n=3, mean ± SD).*

Addition of exogenous cholesterol has been found previously to reverse the effects on infection caused by cholesterol depletion [19]. We investigated whether or not enhancement of infectivity upon partial cholesterol depletion at low [MβCD] could be reversed by replenishment with different sterols, in an experiment analogous to that described above for lytic inactivation recovery. Pseudovirus samples were first treated with 78 μM PBS. After washing out soluble MβCD, virus was mixed with 78 μM cholesterol and then fractionated using an Iodixanol gradient. Virus fractions were collected, and cell infection activities measured were normalized to p24 content. The infectivity measured in the peak p24 fraction is reported in **Figure 14**. As with lytic

inactivation activity, infectivity decreased substantially compared to the magnitude shown by MβCD-treated virus without added cholesterol.

DISCUSSION:

The current investigation was undertaken to evaluate the role of membrane cholesterol depletion on the previously observed potent and specific lytic inactivation of HIV-1 by peptide triazole thiols, such as KR13 [11, 46], that bind to gp120 and trigger release of luminal p24. Prior work [19, 21-23] had already shown that large-scale cholesterol depletion by high concentrations of MβCD (>500 μM) causes HIV-1 disruption and inactivation as judged by gp120 shedding and loss of cell infection activity. Here, we observed a similar loss of lytic inactivation activity at high [MβCD]. However, importantly, we found that low-to-intermediate [MβCD] instead caused a significant enhancement of lytic inactivation (**Figure 5**B). The enhancement effect, which we visualize to occur by "sensitization" of the virus membrane to transformation, occurred in the same [MβCD] dose range at which substantial cholesterol depletion and gp120 shedding occurred (**Figure 7**A and B). The effects of MβCD on lysis were reversed by adding cholesterol. MβCD concentrations causing lytic enhancement also affected membrane lipid bilayer organization (**Figure 12**D) but not fluidity (**Figure 12**C), as judged using membrane-incorporated fluorophores (Dehydroergosterol vs. Laurdan). The enhancement of lysis with partial cholesterol depletion may be related to a decrease in the energy barrier to membrane transformation as judged by the reduced slope in the rate of lysis with vs. without MβCD pre-treatment over a range of temperatures (**Figure 13**A and B). In accord with prior findings [19], an enhancement of virus infectivity was also observed at moderate [MβCD] (Fig. 6), suggesting that common factors are important in

both membrane lysis induced by peptide triazole thiols and fusion occurring in virus-cell infection.

Results obtained in this work argue that cholesterol depletion effects on lysis and infectivity are specific and likely due to alterations in the virus membrane. The ability to reconstitute the functional phenotype of the untreated virus by sterol replenishment after MβCD treatment demonstrates that the MβCD effect is reversible and dependent mainly on sterol content in the virus membrane. The extent of regain of phenotype upon replenishment is dependent on the extent to which the replenishing sterol supports raft formation, consistent with the previously observed importance of rafts for virus infectivity [19]. Further, we confirmed that the virus fractions used in this work were fully depleted in CD45 protein (**Figure 25**) and hence do not contain exosomes that could confound monitoring of biochemical effects due to non-specific release of gp120 or p24 upon MβCD treatments. That the MβCD effects observed in this work are due to specific changes in membrane order fits with the observed correlation of enhancement with changes in the fluorescence of the reporter DHE incorporated into the virus envelope membrane (compare **Figure 12**D and **Figure 5**B).

Enhancement of PTT-induced lysis by concentrations of MβCD that cause Env gp120 shedding is paradoxical, as the Env protein is needed for PTT binding. Importantly, retention of HIV-1 infectivity has been shown before to tolerate reduced gp120 produced

by either enzymatic removal of inactive spikes [52] or lower incorporation of trimer on recombinant virus [67]. Still, the extent of gp120 shedding induced at lysis-enhancing concentrations of MβCD is substantial. One possible explanation for this paradox is that any reduction of lysis due to loss of gp120 is counterbalanced by a reduction of the energy barrier for lytic transformation of the virus particles. This explanation is supported by the observed decrease in slope (which relates to the activation energy) with 78 μM MβCD pre-treatment (**Figure 13**A and B) when 80% of virus-associated gp120 has been shed (**Figure 7**B). The virus spike is known to be metastable, with receptor binding to Env able to drive a cascade of conformational transitions leading from a high energy Env unliganded state to a residual low energy form in which gp41 has formed a 6-helix bundle [45]. Depleting cholesterol could lower the energy barrier to gp41 6-helix bundle formation, which has been found previously to be a component not only of the entry/infection process [45] but also of the lysis process [11]. This hypothetically could occur because cholesterol can act as a stabilizing agent, locally increasing lipid density around the spike in raft domains and keeping it stable. This stabilizing behavior has been observed for other proteins with membrane spanning domains such as CCR5 [68], β2 Adrenergic receptor [69], Serotonin 1A receptor [70] and the Oxytocin receptor [71]. The fact that the cholesterol content on the native virus does not result in the most sensitized state of the spike is noteworthy. In this view, depletion of cholesterol with MβCD would result in a more unstable Env spike, which would be more vulnerable to ligand-induced rearrangement, shedding and perturbation of associated membrane. Hence, the cholesterol content found on the native virus strikes a balance between stability and transformability of the virus spike, as depicted in **Figure 16**.

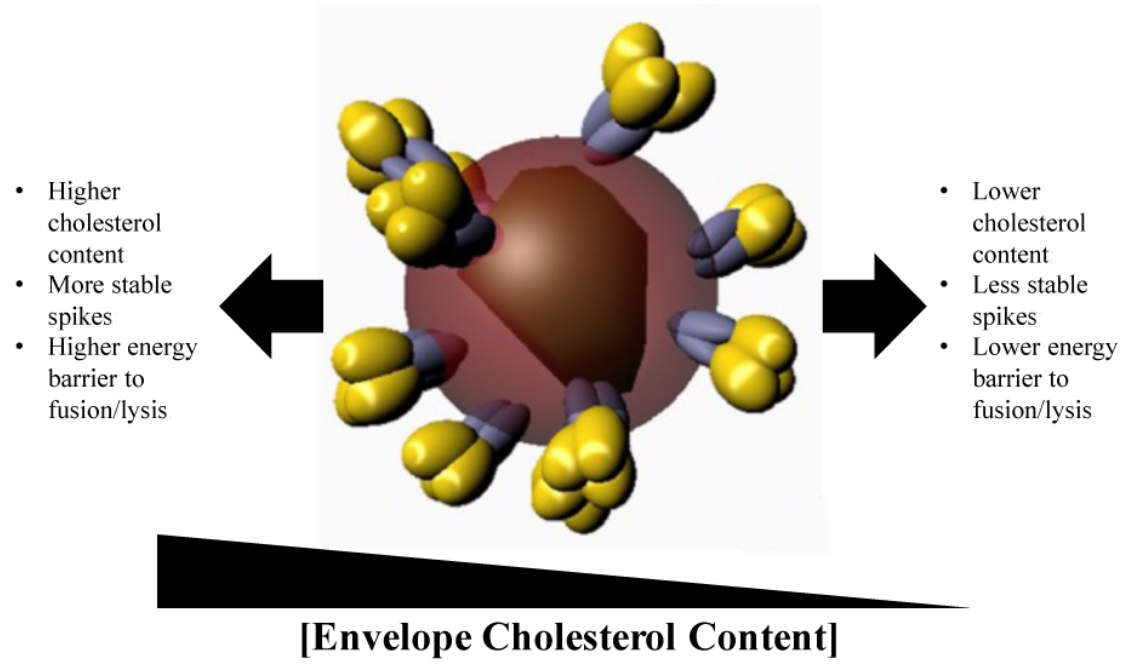

Figure 16: *Rationale for how HIV-1 envelope cholesterol content helps strike a balance between stability of the spike at higher cholesterol content and transformability at lower cholesterol content.*

*We found in this work that enhancement of ligand-induced virus lysis at intermediate cholesterol depletion correlates with infectivity enhancement, a phenomenon that has been observed previously [19] and amplified in the current study. The extent of MβCD dose dependence and sterol replenishment are similar for both lysis and infectivity. Of note, the magnitude of infectivity enhancement previously reported to occur at elevated MβCD was lower than that observed in the current study. The quantitative differences in the extent of infectivity enhancement in this and prior work may be due to use of different viruses, as shown here by differences with BaL01, YU2 and JR-FL pseudotypes (**Figure 14** vs.*

Figure 15C). As with lysis (discussed above), infectivity enhancement by MβCD concentrations that decrease the amount of gp120 presents a paradox of increased function in the face of decrease in the Env spike required for function. We envision that the lower energy barrier effect found here for lysis would also explain increased infectivity with virus containing reduced gp120. This fits with the previously observed finding that lysis and infection have mechanistic similarities, including a role for gp41 6-helix bundle formation in both processes [11].

The observations made in the current work, that cholesterol depletion can trigger changes in membrane properties leading to either functional enhancement or suppression depending on the extent of depletion, can be related to other Type I enveloped viruses, including Influenza, Ebola and Dengue, which have high cholesterol contents and depend on membrane transformation mechanisms to effect virus-cell membrane fusion and cellular infection [12, 14, 17, 18, 47, 48]. For example, a bell-shaped effect of cholesterol depletion on biophysical properties of liposomal fusion and content mixing rates for influenza virus has been reported [48]. Hence, defining the nature of membrane transformations that occur in enhancement of function caused by cholesterol depletion in HIV-1, including how these transformations are associated with Env spike protein, could help improve understanding of fusion mechanism for Type I viruses generally. Such studies also could help in understanding the nature of membrane transformations triggered by Env protein ligands such as KR-13, and in turn how such lytic ligands could serve as prototypes to define strategies for virus neutralization by harnessing the vulnerabilities of enveloped virus membranes.

Chapter 3: Role of Spike gp41 in Lytic Release of p24 and Infectivity

INTRODUCTION:

The structural and functional characteristics of gp41 sequence domains have been evaluated extensively by antibody inhibition studies, mutagenesis and peptide mimics. Recent structures obtained via crystallography and cryo-TEM on SOSIP proteins have enhanced our understanding of gp41 structure within the context of a native-like spike [72, 73]. This body of literature comes to our aid when we need to understand the structure of different regions of the ectodomain of gp41 that target the membrane.

REGIONS OF INTEREST WITHIN GP41:

CRAC region within MPER: This region involves 5 amino acids (LWYIK) that are >98% conserved (Los Alamos National Labs). Peptide mimics of this region are capable of binding to cholesterol molecules, and in liposome studies, can cause cholesterol to aggregate out of the membrane and form crystals in local regions surrounding the peptide [36]. The single mutation that has the most suppression of these abilities is a Leu to Ile mutation though a clear explanation for such a small change having a big effect is not

known [38]. All mutations have been shown to have a drop in infectivity as compared to wild type and may affect lysis since they don't interact as well with cholesterol.

C-terminal tail of gp41: The C-terminal tail of gp41 found in the viral lumen has not been characterized as much in terms of structure or function. Regions of the protein termed as lentiviral lytic peptides have been named thus due to the activity of peptides that mimic the sequence [42]. It has been shown that truncating the tail completely results in greater incorporation of spikes in viruses. It also results in either a drop or increase in infectivity depending on which strain of HIV-1 virus is tested. Truncating the tail might result in a loss in lysis with PTT if the tail is involved in the lytic mechanism. The truncation is accomplished by introducing a stop codon at the first cytoplasmic residue. If this is found to affect lysis, further mutations can be tested which allow differential lengths of the tail to exist.

TM domain mid-span arginine: The mid-span region of gp41 consists of hydrophobic amino acids since the sequence domain traverses a hydrophobic region of the bilayer. However, it has a single polar amino acid in the middle (mid-span arginine). This residue is >99% conserved within HIV-1 sequences (Los Alamos National Labs) and is also found in other viruses and is hypothesized to thin the membrane either through the formation of a water cavity within the bilayer or by interacting with phospholipid head groups on the inner layer [39, 41]. Either way, it has been shown computationally to reduce the energy required to further thin the membrane and disrupt it. Mutations that replace this polar

residue with a hydrophobic residue such as Ala for Arg may result in the de-thinning of the membrane at the viral spike and suppress lysis from taking place.

MPER tryptophans: There are five tryptophans that are spread out over the MPER sequence. A comprehensive survey of the literature suggests these residues are crucial for infection. Prior work has demonstrated that individual mutations have little effect on viral infectivity but combined mutations starting from the N-terminus have large suppressive effects on infectivity [32, 33]. Hence, the plan is to mutate Tryp residues to Ala and develop three mutants: W(1-5)A which consists of all 5 residues mutated; W(1-3)A which has only the first three (N-terminal) Trp residues mutated; and W(4-5)A which consists the last two (C-terminal) Tryp residues mutated. The first mutant is an all/nothing mutation that should have the biggest effect. The second and third mutants will help in locating the region of MPER most responsible for lysis.

gp120 Stabilization: Since prior work has demonstrated that gp120 is shed during the depletion of cholesterol, the literature was surveyed for mutations that stabilized gp120 within the trimeric spike thereby potentially reducing the amount of gp120 being shed. If shedding of gp120 were reduced, it would answer the question as to whether shedding were a requirement for the bell-shaped trend observed or a consequence of the transformations taking place. If shedding were reduced, the number of functional spikes capable of participating in lysis at increasing amounts of MβCD, which might fundamentally alter the bell-shaped trend observed with wild-type virus. The mutation that has been studied in

literature that has reduced shedding is one in gp120 that substitutes an Asn for a His [74, 75]. This mutant is resistant to shedding with the addition of CD4. Since CD4 and peptide triazoles have different binding sites and potentially induce different conformational changes within gp120, the mutant might not remain resistant to shedding and it remains to be tested.

MATERIALS AND METHODS:

Plasmids encoding BaL.01 gp160 and NL4-3 Luc^+ R^- Env^- were obtained from the NIH AIDS Reagent Program as a kind gift from Dr. John Mascola and Dr. Nathaniel Landau respectively. Primers to perform mutations were designed and then ordered from IDT Tech.

PEPTIDE TRIAZOLE SYNTHESIS AND VALIDATION:

Peptides were synthesized as described before [9, 49] by stepwise solid-phase peptide synthesis on a Rink amide resin with a substitution value of 0.25 $mmolg^{-1}$ (Novabiochem). All Fmoc-amino acid derivatives and coupling reagents were purchased from Chem-Impex International Inc. Synthesis-grade solvents were used in all procedures. All peptides were purified to 98% homogeneity as judged by analytical reversed-phase HPLC on C18. The

integrity of purified peptides was confirmed by MALDI-TOF mass spectrometry; observed mass was 2085.43 Da vs. 2085.19 Da expected for KR-. Peptide triazole thiol KR-13 was solubilized in 1x PBS, pH 7.2 and the absorbance measured at 280 nm with a quartz cuvette in a Shimadzu UV1700 spectrophotometer. The concentrations were determined using extinction coefficient of 6090 $M^{-1}cm^{-1}$ for KR-13. The functionality of the peptide was tested by CD4 and 17b competition assays using surface plasmon resonance (SPR) analysis with a Biacore 3000 optical biosensor.

SITE DIRECTED MUTAGENESIS:

Mutations to the BaL.01 plasmid were introduced using the protocol from Qiagen. Reagents used were purchased from New England Biolabs. Briefly, a 50 µl mix of 200 nM of the forward and reverse primers was mixed with 5 µL of 10x PfuUltra buffer, 0.4 ng/µL template DNA, 1 µL of 10 mM DNTP mix and 1 µL of PfuUltra enzyme was made and then run on an Eppendorf thermal cycler. The PCR product was then subjected to a 2 hour digest at 37 °C with DpnI to remove the template DNA. The mixture was then transformed into XL-10 Gold ultracompetent bacteria and grown overnight on agar plates using Ampicillin as a resistance antibiotic. Colonies were picked the following day and grown in a 3 ml culture overnight and then mini-prepped (Promega) to extract the DNA. The DNA was quantified and then sent for sequencing to Genewiz. Once the mutation was

confirmed, the DNA was transformed into Stbl2 bacterial cells and grown in 500 ml cultures overnight and maxi-prepped (Qiagen) to extract transfection-grade DNA.

For the mutations performed, all residue positions are numbered with respect to the BaL.01 sequence. V2E (V510E) was made using the forward primer: 5'-AGA AAA AAG AGC AGA GGG AAT AGG AGC TGT – 3' and the reverse primer: 5' – ACA GCT CCT ATT CCC TCT GCT CTT TTT TCT- 3'. The C-tail truncation mutant was made by introducing a stop codon at residue Arg 706 with the forward primer: 5' – GAA TAG AGT TTA GCA GGG ATA CTC ACC ATT ATC – 3' and the reverse primer: 5' – GAT AAT GGT GAG TAT CCC TGC TAA ACT CTA TTC – 3'. The CRAC mutant was made by substituting Leu 676 with Ile with the forward primer: 5' – CAA AAT GGA TCT GGT ATA TAA AAA TAT TC – 3' and the reverse primer: 5' – GAA TAT TTT TAT ATA CCA GAT CCA TTT TG – 3'. The MPER mutations were performed sequentially. W1 = 663, W2 = 667, W3 = 669, W4 = 675, W5 = 677. W(1)A was made with the forward primer: 5' – TAT TAG AAT TAG ATA AAG CGG CAA GTT TGT GG – 3' and the reverse primer: 5' – CCA CAA ACT TGC CGC TTT ATC TAA TTC TAA TA – 3'. W(1-2)A was made with the forward primer: 5' – ATT AGA TAA AGC GGC AAG TTT GGC GAA TTG GTT TGA CAT AAC – 3' and the reverse primer: 5' – GTT ATG TCA AAC CAA TTC GCC AAA CTT GCC GCT TTA TCT AAT – 3'. W(1-3)A was made with the forward primer: 5' – GAA TTA GAT AAA GCG GCA AGT TTG GCG AAT GCG TTT GAC ATA AC – 3' and the reverse primer: 5' – GTT ATG TCA AAC GCA TTC GCC AAA CTT GCC GCT TTA TCT AAT TC – 3'. W(4)A was made with the forward primer: 5' –

GAC ATA ACA AAA GCG TAT ATA AAA ATA TTC ATA ATG ATA GTA GGA G – 3' and the reverse primer: 5' – CTC CTA CTA TCA TTA TGA ATA TTT TTA TAT ACG CCA GCG CTT TTG TTA TGT C – 3'. W(4-5)A was made with the forward primer: 5' – GAC ATA ACA AAA TGG CTG GCG TAT ATA AAA ATA TTC ATA ATG ATA GTA GG – 3' and the reverse primer: 5' – CCT ACT ATC ATT ATG AAT ATT TTT ATA TAC GCC AGC CAT TTT GTT ATG TC – 3'. The W(1-5)A mutant was made sequentially after making W(1-3)A using the W(4-5)A primers. The primers and mutations for the TM and shedding mutant were designed and performed by Andrew Holmes. The TM mutant was created by substituting Arg 696 with Ala using the forward primer: 5' – GCT TGA TAG GTT TAG CAA TAG TTT TTT CTG – 3' and the reverse primer: 5' – CAG AAA AAA CTA TTG CTA AAC CTA TCA AGC - 3'. The shedding mutant was created by substituting His 66 with Asn using the forward primer: 5' – GAT ACA GAG GTA AAT AAT GTT TGG G – 3' and the reverse primer: 5' – CCC AAA CAT TAT TTA CCT CTG TAT C - 3'.

PRODUCTION AND CHARACTERIZATION OF PSEUDOVIRUSES:

Pseudoviruses were made as described in Chapter 2. Briefly, 3 million cells were seeded in a T-75 flask (Corning) the day before transfections. DNA expressing the spike BaL.01 gp160 or the mutant was co-transfected (4 μg) with the plasmid expressing the core (NL4-3, Luc+R-E-, 8 μg) using polyethyleneimine as a transfection vehicle. The growth medium

was changed 24 hours post-transfection and the supernatants collected 72 hours post-transfection. The supernatant was concentrated using a 100 kDa MWCO concentrator (Amicon, EMD Millipore) and loaded on an Optiprep gradient from 6% to 20% diluted in serum free media. The samples were spun for two hours at 110,000 x g at 4 °C and then the fractions containing the virus were pooled and aliquoted before being frozen at -80 °C.

Pseudoviruses were characterized for infectivity, gp120 incorporation and normalized based on their p24 content. Infectivity assays were performed on HOS.T4.R5 cells using chemiluminescent signal from Luciferase activity as an end point readout. gp120 incorporation was measured by running viral lysate on a western blot. p24 content was measured using a sandwich ELISA with a standard curve that allowed for quantification.

LYSIS OF MUTANTS WITH PTT (KR-13)

Lysis profiles were created by treating each mutant to a range of concentrations of the PTT starting from 100 μM. Mutants, tittered for infectivity and p24 content immediately after production, were diluted such that 50 ng/ml (p24 content) was the final concentration loaded onto the plate. Samples were mixed through six inversions and incubated at 37 °C for 30 minutes before being spun down to pellet viral debris at 21,130 x g for two hours at 4 °C on a table top centrifuge (Eppendorf). The top 100 μl was collected from each tube and mixed (1:1, v/v) with PBS containing 1% BSA and 0.1% TX-100 before being loaded

onto an ELISA plate that had been pre-coated with Mouse anti-p24 (Abcam) and blocked. Samples were allowed to bind overnight before being washed and stained with Rabbit anti-p24 (Abcam, binds to an unknown but different epitope from the Mouse antibody) and a Donkey anti-Rabbit conjugated to HRP for 1 hour each. End point results were generated colorimetrically using Sodium Citrate with Perborate as a substrate and Orthophenylenediamine (OPD) as a color changer. Every mutant tested had a positive control (+ 0.1% TX-100) and a negative control (PBS, no PTT) that allowed the calculation of the lysis profile.

For cholesterol depletion assays, samples of virus were first treated with a serial dilution of MβCD, starting at 5000 μM for 30 minutes at 37 °C followed by 5 μM KR-13 for another 30 minutes at 37 °C before being spun to separate the released protein from the viral pellet. The rest of the assay was run as above.

RESULTS:

MUTANT EXPRESSION AND CHARACTERIZATION

All mutants were produced in HEK-293T cells and purified on a 6-20% Iodixanol (SigmaAldrich) gradient. Once they were purified, all mutants were titered for infectivity, gp120 content and normalized using p24 content. As the data show in Figure 17, all mutants had differing levels of infectivity. The CRAC mutant and the MPER mutants had the least infectivity while the tail deletion mutant, the spike stabilization mutant and the TM mutant had intermediate levels of infectivity which were all consistent with prior literature. All mutants had comparable levels of gp120 incorporation.

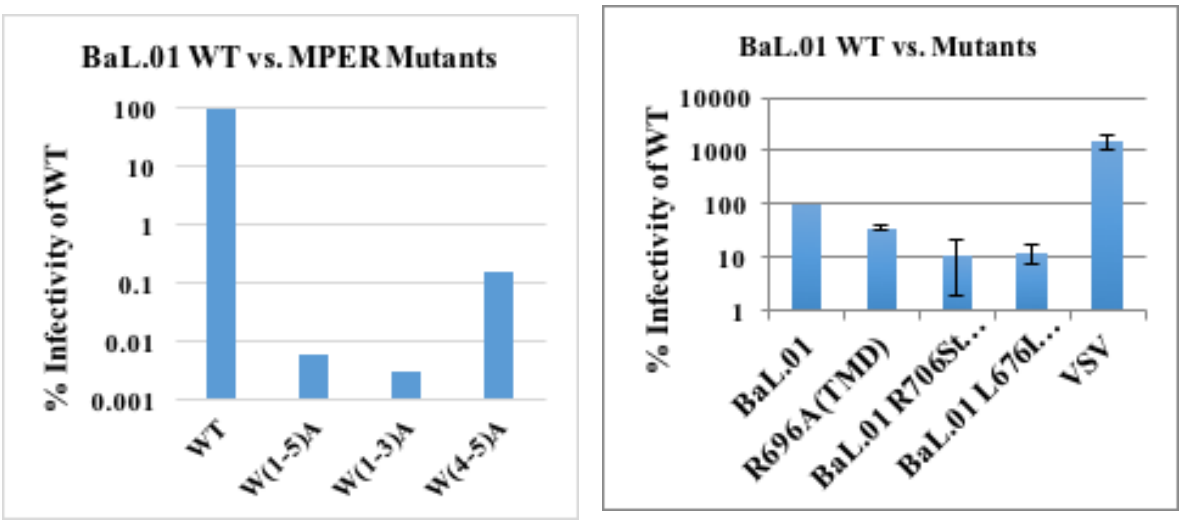

Figure 17: *Characterization of BaL.01 mutant infectivity after being normalized for p24 content. (A) MPER mutants compared to wild-type. (B) CRAC, Tail truncation, TM and H66N mutants compared to wild-type*

PTT KR-13 CAUSES LYTIC RELEASE FROM MUTANTS TARGETING LIPID INTERACTING REGIONS OF GP41

The PTT KR-13 has been shown to lyse BaL.01 pseudotyped virus (IC_{50} ~ 5 µM). The question asked was whether mutants that affected the interaction of the virus spike protein gp41 with the viral envelope membrane would still be lysed. Mutations were performed on the BaL.01 gp160 plasmid and the mutations, once confirmed, were expressed as mutant pseudotyped viruses. Mutations targeted cholesterol interaction at the C-terminus of MPER (L676I in the CRAC sequence), the C-terminal tail with a stop codon (R706Stop),

membrane thinning with the mid-span Arginine (R696A), MPER interaction with the membrane (W(1-5)A, W(1-3)A and W(4-5)A) and spike stabilization (H66N). Mutants were treated with KR-13 and then spun to pellet virus debris before the supernatant was tested via sandwich ELISA for p24 content.

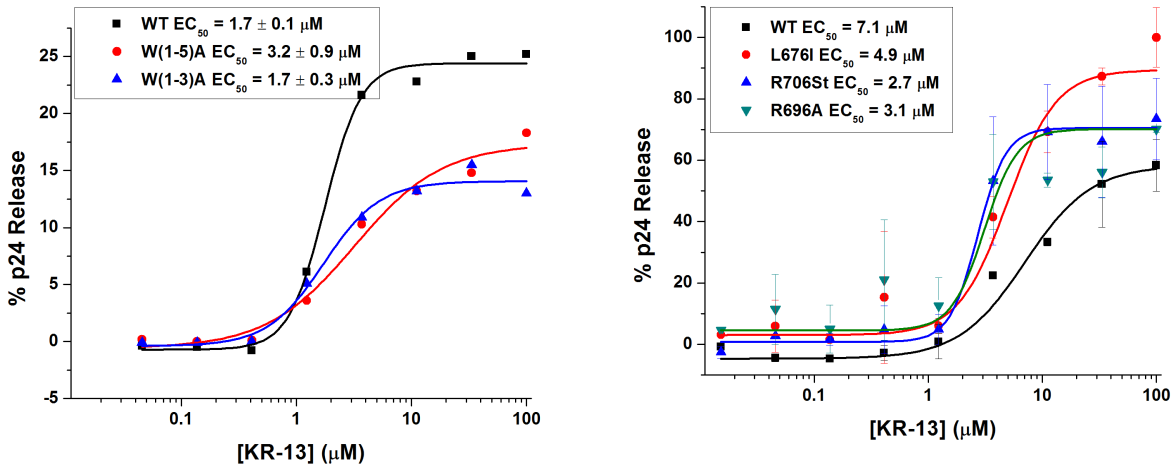

Figure 18: *KR-13 dose profiles for BaL.01 pseudotyped wild-type and mutant viruses*

The data from Figure 18 (A and B) show that all mutants exhibit a dose-dependent lytic release when treated with KR-13. While the EC_{50}s vary between the mutants tested, the differences in estimated EC_{50}s are relatively small.

MUTATIONS TARGETING MPER REGION OF GP41 HAVE DIFFERING SENSITIVITIES TO CHOLESTEROL DEPLETION

Of the mutants characterized above, MPER mutants were tested for their sensitivity to cholesterol depletion with a lysis assay as done previously in Chapter 2. Briefly, each mutant was treated with a dose range of MβCD starting from 5000 μM for 30 minutes at 37 °C followed by 5 μM KR-13 for another 30 minutes at 37 °C. As a control, a sample of each mutant was treated with PBS followed by KR-13 to get the base-line lysis. After the 30 minute treatment with KR-13, all the samples were spun on a table top centrifuge at 21,130 x g for 2 hours at 4 °C. The supernatants were collected and tested for the presence of p24 protein. The data suggest that the mutants show differing levels of sensitivity.

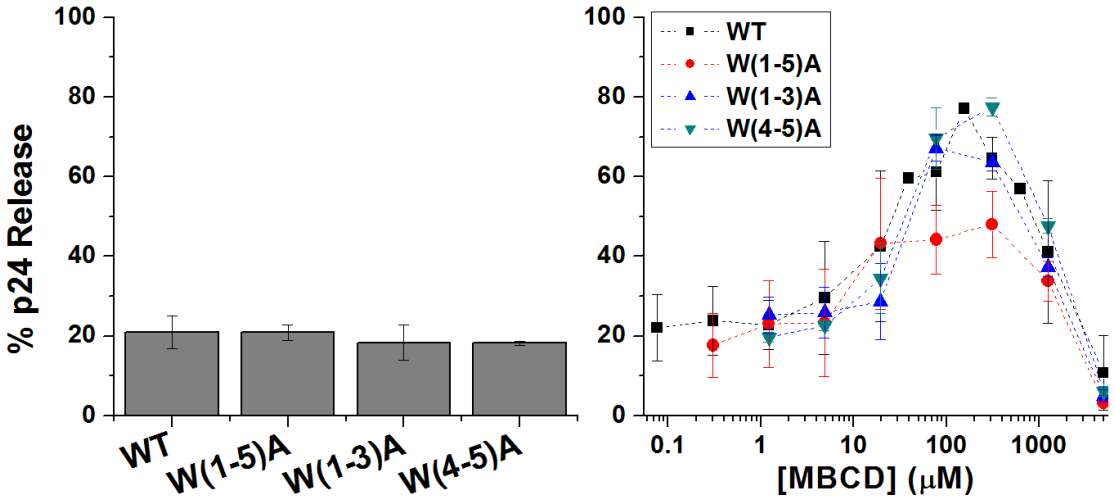

Figure 19: *Lytic Release from WT and MPER Tryptophan Mutants. (A) Base-line release of capsid p24 after treatment with PBS for 30 minutes at 37 °C followed by 5 μM KR-13. (B) Release of capsid p24 after pre-treatment with MβCD for 30 minutes at 37 °C followed by 30 minutes with 5 μM KR-13 for WT (black squares), W(1-5)A (red circles), W(1-3)A (blue upright triangles) and W(4-5)A (greed downward facing triangles).*

In Figure 19, the lytic release from tryptophan mutants with PTT were compared with WT. In Figure 19A, the base line lysis observed with KR-13 was similar between all three mutants and wild type. In Figure 19B, the maximum enhancement observed was with the W(4-5)A mutant (green, 80%) and the least was with the W(1-5)A mutant (red, 50%). The W(1-3)A mutant (blue, 70%) as expected fell in between the two though it was closer to W(4-5)A and WT. The difference in behaviors observed with MPER mutants suggest sensitization observed with lysis after cholesterol depletion depends on the trp residues, though the exact role is unknown.

MUTATIONS TARGETING PUTATIVE CHOLESTEROL BINDING REGIONS OF GP41 ALTER SENSITIVITY TO CHOLESTEROL DEPLETION

Pseudoviruses expressing mutations targeting cholesterol-binding regions of gp41 were next tested for their sensitivity to cholesterol depletion with lysis.

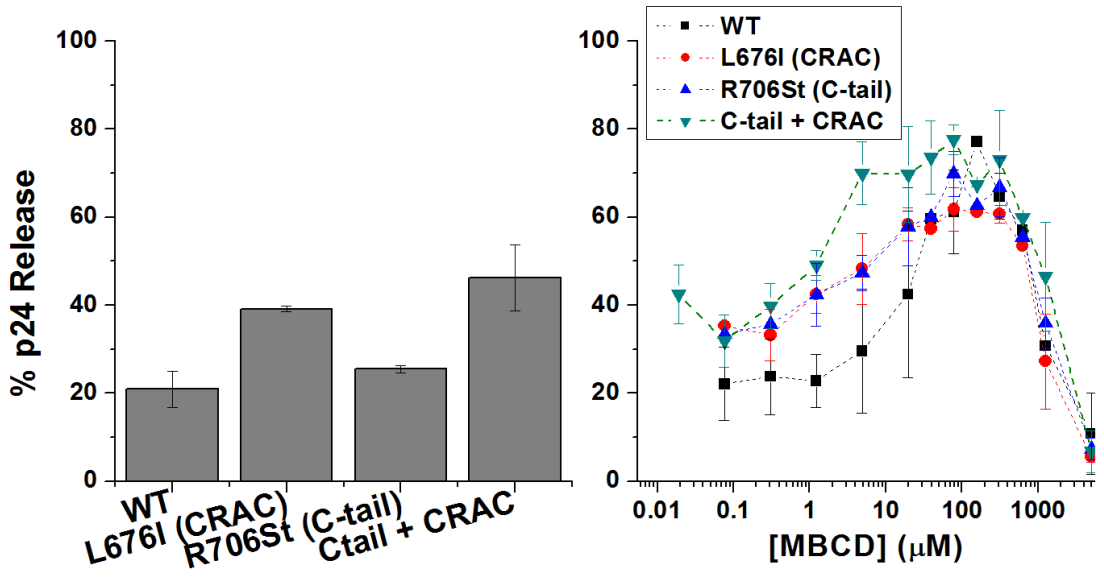

Figure 20: *Lytic Release from CRAC, C-tail truncation, and a double mutation incorporating both compared to WT. (A) Base-line release of capsid p24 after 30 minutes treatment with PBS at 37 °C followed by 30 minutes treatment with 5 μM KR-13 at 37 °C. (B) Release of capsid p24 after 30 minutes treatment with MβCD at 37 °C followed by 30 minutes treatment with 5 μM KR-13 at 37 °C from WT (black squares), L676I (red circles), R706St (upright blue triangles and the double mutant, C-tail + CRAC (downward green triangles).*

In Figure 20, mutants targeting cholesterol-binding regions were compared. Figure 20A shows the base-line lysis between the mutants. Surprisingly, the L676I (CRAC) mutant and the double mutant showed enhanced baseline lysis (**Figure 20**A) compared to WT and the C-tail mutant (*ca* 40% compared to 20 and 25% respectively). In Figure 20B, the lytic trend with KR-13 showed both the CRAC (L676I, red circles) and C-terminal tail truncation mutants (R706St, blue upright triangles) having enhanced lysis at low [MβCD] (< 10 μM) while the WT pseudovirus does not show enhanced lysis at higher [MβCD] (> 10 μM). Additionally, the maximum lysis for the L676I and the R706St mutants was lower than either WT or the double mutant. Possibly the more significant interpretation of these

data is that the cholesterol-binding mutants all showed diminished total change in lysis from base line to the maxima with the L676I and R706St mutants having the least.

MUTATIONS TARGETING TM AND GP120 DO NOT AFFECT LYSIS OR SENSITIVITY TO CHOLESTEROL

The two remaining mutants (R696A, TM) and H66N were tested. These mutants were not targeting cholesterol binding and hence were not expected to be different from WT.

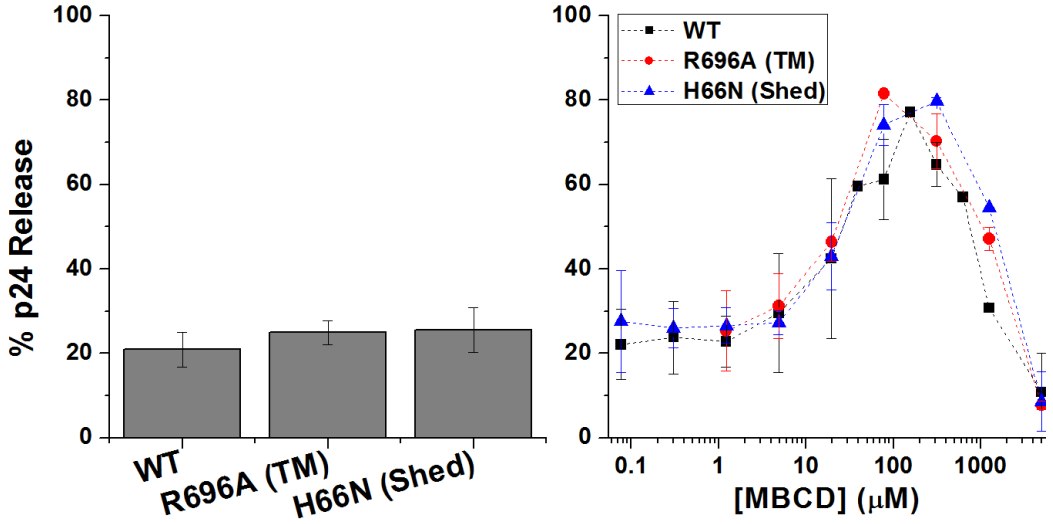

Figure 21: *Lytic Release from WT, R696A (TM) and H66N (shedding resistant) mutants. (A) Base-line release of capsid p24 after 30 minutes treatment with PBS at 37 °C followed by 30 minutes treatment with 5 μM KR-13 at 37 °C. (B) Release of capsid p24 after 30 minutes treatment with MβCD at 37 °C followed by 30 minutes treatment with 5 μM KR-13 at 37 °C from WT (black squares), R696A (red circles) and H66N (upright blue triangles).*

As shown in **Figure 21**A and B, the trends observed with TM mutant (R696A, blue) and gp120 mutant (H66N, green) show no difference from the trend of WT (black squares) with cholesterol depletion, further confirming that differences are only observed with mutations targeting specific regions of gp41.

DISCUSSION:

Cholesterol is the most abundant constituent of viral lipid bilayers (*ca*. 45 mol %) [12, 14, 47] and yet there is no definitive function attributed to it. It has been hypothesized to bind to proteins containing segments known as CRAC domains based on calorimetry work done on pentapeptide sequences that mimic these domains [76, 77]. It has also been suggested that cholesterol acts as a packing factor, stabilizing membranes with high radii of curvature such as the viral envelope and complex membrane-bound proteins where conformation may be hard to maintain without membrane-imposed stability [78-80]. This might be important for the virus spike which is a high energy hexamer of proteins held together non-covalently. In fact, the cholesterol content surrounding spikes is thought to increase as the spike makes its way as an uncleaved protein from the endoplasmic reticulum in membranes with low cholesterol content to the cell surface where it has been cleaved and has become

metastable but is surrounded by high cholesterol content in lipid rafts from which it buds off as shown in **Figure 22** [81, 82].

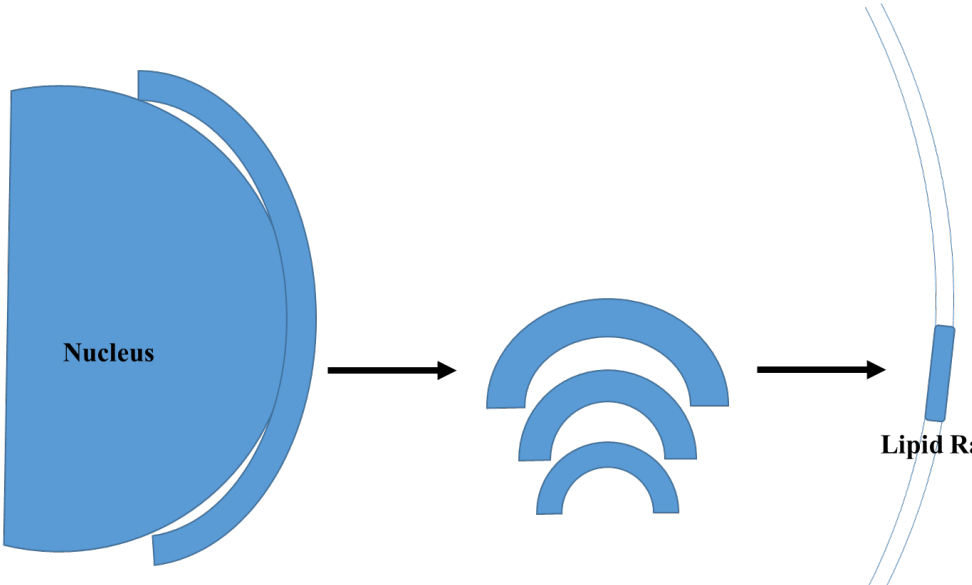

	Endoplasmic Reticulum	Golgi Body	Plasma Membrane
Cholesterol Content	**13%**	**16.7%**	**50%**

***Figure 22**: Changes in cholesterol content in lipid bilayers traversed by gp160 protein from synthesis in the endoplasmic reticulum to virion incorporation at the plasma membrane of cells. Cholesterol content increases gradually from ~ 13% at the endoplasmic reticulum to ~16.7% in the golgi to ~50% in the plasma membrane. Cholesterol quantification from [82]*

This might suggest that envelope cholesterol that tightly packs around the spike acts to create an energy barrier to stop the spike from conformational rearrangements that might result in inactivating it. This energy barrier created by cholesterol would also hinder conformational changes required to undergo productive infection or lysis with PTTs. When cholesterol is depleted with the use of MβCD, there is less cholesterol present to

pack with the spike and this reduces the energy barrier. It might explain the enhancement seen in lysis and infection. Since the CRAC pentapeptides have been shown to bind cholesterol and the CRAC mutant peptide does not, we can hypothesize that the CRAC mutation in the virus might similarly reduce the affinity of gp41 CRAC for cholesterol. The same goes for the mutation that truncates the tail domain since this region is believed to interact with cholesterol within the inner bilayer leaflet. While MβCD-based depletion happens only on the outer leaflet, it is thought that cholesterol located on the inner-leaflet flips to the outer leaflet to maintain the asymmetry between the leaflets. It has been shown computationally with model membranes [62, 83] and with wet lab experiments [84] that in membranes with rafts, depletion of cholesterol begins in non-raft regions (fast pools, $t_{½}$ = 19~23 seconds, [84]), where the sterol has a lower affinity to remain in the membrane, followed by raft regions (slow pools, $t_{½}$ = 15~30 minutes, [84]). Based on prior literature on the behavior of CRAC peptides and our mutational data, we hypothesize that the presence of spike gp41 segments carrying the CRAC sequence enhance the area of the "slow pools". Hence, when the spike gp41 is mutated to have a lower affinity for the envelope cholesterol (e.g. L676I or R706St mutant), it can be assumed that sterols are more readily depleted from raft pools with agents such as MβCD, resulting in a lower amount of the depletion agent needed to sensitize the virus as observed in Figure 20B with the L676I and R706St mutants.

While the CRAC domain might be responsible for cholesterol interaction, the rest of the MPER domain might have a different function. The most potent mutational modifications

of MPER that lead to the largest drops in infectivity had to do with replacing all or the first three highly conserved tryptophans **Figure 17**A and [32, 33, 85, 86]. Even substituting tryptophan with alanine, an alternate hydrophobic residue still results in near complete loss of infectivity. Such trends might be important for other enveloped viruses such as Influenza [87] and Ebola [88], which have similar MPER domains. MPER is also exposed after KR-13 treatment, and preliminary data (not shown) suggested MPER antibody 10E8 competed out lysis. Mutants in the MPER region showed little or no infectivity (**Figure 17**), though they expressed well and had nominal amount of spike gp120 incorporation, consistent with literature. When tested for lysis however, they turned out to be similar to the wild-type virus (lytic IC_{50} with PTT, **Figure 18**B). However, differences were revealed when the mutants were tested for sensitivity to cholesterol depletion (Figure 19B). W(1-5)A and W(1-3)A both had reduced sensitization with cholesterol depletion while W(4-5)A was close to wild type pseudovirus. The first three tryp residues are shown to be the most important in affecting infection while the last two (W(4-5)) have a smaller effect. While lysis with KR-13 was not completely aborted with the MPER mutations, a pattern of suppression emerged that was consistent with prior literature on infectivity. Based on these observations, one could argue that either (1) MPER domain participates directly in lysis and cholesterol interactions, or (2) MPER domain participation is indirect in messaging from cholesterol to lysis, such as stability of the spike and/or 6-helix bundle formation. However, it is clear that while lysis and fusion share many events, they have different sensitivities to protein changes.

Chapter 4: Data Interpretation and Future Directions

The over-arching goal of this thesis was to shed light on the role of the lipid bilayer and the embedded spike gp41 protein in the lysis event triggered by PTTs like KR-13. The benefits to pursuing PTTs are multi-fold:

1. PTTs are potent, sub-micromolar inhibitors of HIV-1 entry with dual antagonist behavior against CD4 and co-receptor, shedding of spike gp120 and lytic release of capsid p24, the latter two of which are irreversible in their inactivation of the virus. There is a pressing need for such entry inhibitors and understanding the mechanism of inhibition would help develop a powerful class of inhibitors including small molecules and peptidomimetics that share similar attributes.
2. PTTs have been shown to expose previously occluded, highly neutralizing epitopes on MPER, making post-treatment residual virions ideal vaccine candidates.
3. Of all that has been determined about HIV-1, the mechanism of fusion remains a black box. While the events that precede it as well as the events that follow it have been determined, the actual mechanism of fusion remains unknown. This has limited the targeting of HIV-1 entry to (1) targeting the spike proteins, gp120 and gp41, which are either conformationally dynamic, shielded by glycans and mutationally plastic or (2) targeting the membrane which is difficult since viral membranes come from infected cells making them very similar. Since the response

of HIV-1 to PTTs mimics aspects of fusion, studying PTTs could advance our understanding of the fusion mechanism

This thesis set out to uncover the role of lipids and spike proteins and their interplay and while it has fostered new understanding, there are still things to be achieved.

DATA INTERPRETATION:

The data presented in the thesis can help determine an important mechanism taking place at the virological synapse that is affected by lipid composition (Chapter 2) and spike sequence (Chapter 3). These data however require the consideration of caveats.

CAVEATS

Below is a discussion of key pieces of data that are considered in this analysis.

1. MβCD-depletion of cholesterol has resulted in a dose-dependent enhancement in lysis observed with PTT (**Figure 5**B) and infectivity (**Figure 14**). One worry is that MβCD might interact directly with the membranes or proteins to cause this effect. We have assuaged concerns by washing samples with buffer thoroughly or

run samples through a gradient purification method, after MβCD treatment for infectivity assays. In addition, a thorough survey of literature suggests MβCD is specific for cholesterol [89] and does not bind to or interact with lipid bilayers without interacting with cholesterol [90, 91]. Also, observations (**Figure 10**, **Figure 11** and **Figure 14**) indicate that the trends in lysis and infectivity observed with MβCD can be reversed with supplementation of exogenous cholesterol, suggesting that the observed trends in lysis and infectivity have to do with cholesterol and not MβCD.

The sensitization effects on lysis were also seen in an alternate assay in the absence of MβCD, albeit attenuated, where envelope sphingomyelin (SM) was cleaved to produce ceramide.

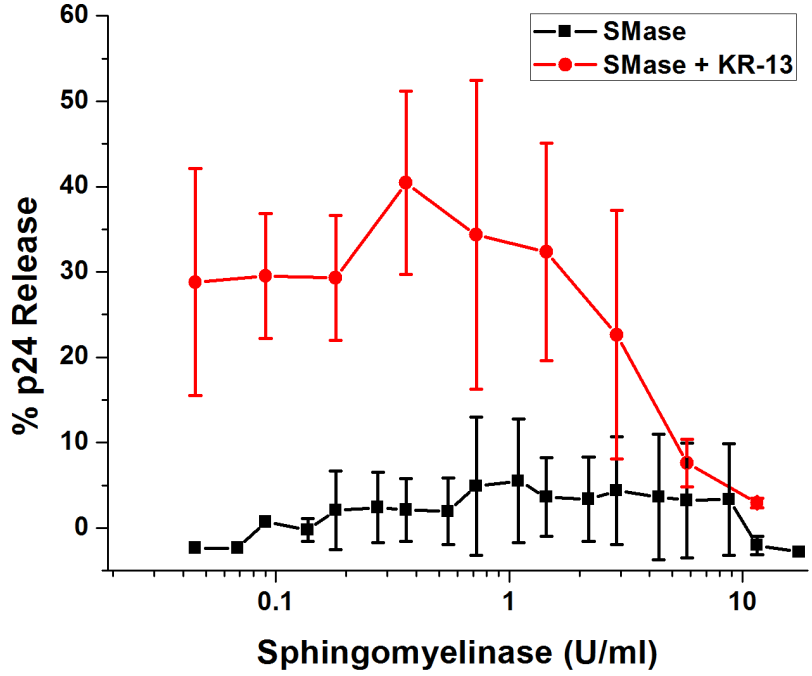

Figure 23: *Lytic release of p24 with SMase treatment (black squares) and SMase treatment followed by PTT treatment (red circles).*

In this assay, the removal of the phosphorylcholine head group with the enzyme Sphingomyelinase is believed to reduce the interaction between SM amide groups and the hydroxyl head groups of cholesterol [92, 93]. Breaking of the interactions between SM and cholesterol was also achieved in an alternate way whereby envelope cholesterol in the outer leaflet was converted to 4-cholesten-3-one with the addition of cholesterol oxidase [94]. This conversion breaks the interaction between cholesterol and SM and possibly the interactions that are required for raft formations [95].

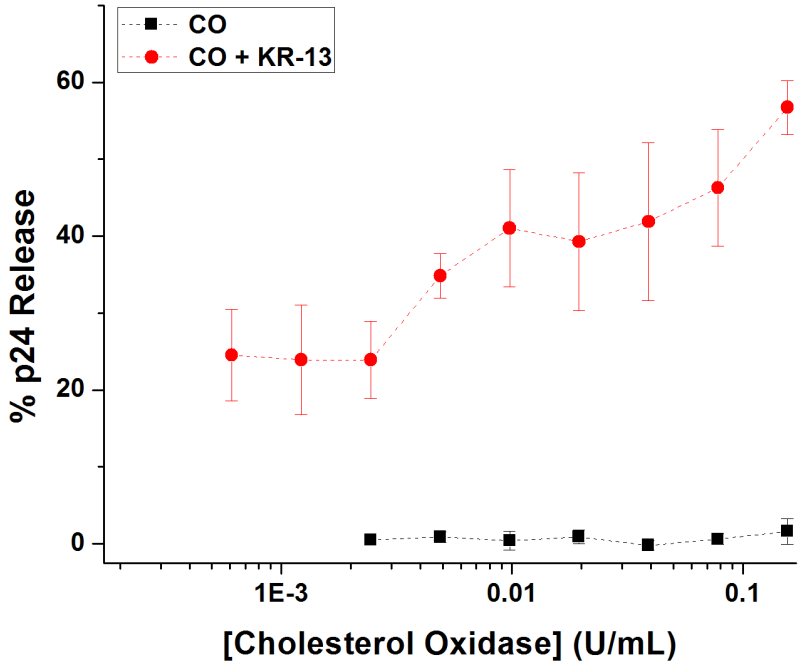

Figure 24: *Impact of Cholesterol Oxidase (CO) pre-treatment on lytic release with PTT on HIV-1 pseudoviruses. Samples of BaL.01 HIV-1 pseudoviruses were treated with a range of serially diluted CO for 30 minutes at 37C and then treated with equal volumes of PBS (black squares) or 5 μM KR-13 (red circles) for another 30 minutes at 37C before spinning to pellet virus debris. Supernatants were tested for p24 content via sandwich ELISA*

The treatment with Cholesterol Oxidase results in an enhancement of lysis from 25% (base-line) to 57% (**Figure 24**). The SMase and CO treatments suggest that the breaking of cholesterol/sphingomyelin interactions is a major effector of enhancement of lysis. These data coupled with sterol reversal of MβCD-mediated depletion argue for cholesterol being the causative agent in the observed sensitization rather than MβCD.

2. Sensitization data presented in **Figure 14** suggest that a small amount of MβCD-depletion of envelope cholesterol enhances the infectivity of HIV-1 pseudoviruses.

This has not been reported in prior literature. Depletion of cholesterol (with large amounts of MβCD > 312 μM) has been associated with a fall in infectivity, whether the treatments were done on cells producing virus or on the viruses themselves [19, 21-23], but depletion with smaller amounts has never been reported. One possibility for the difference in results might have to do with exosomes. These are lipid particles put out by cells that present antigens on their surface depending on the state of the cell they bud from [96, 97]. They are difficult to differentiate from viruses since their size ranges form 30-100 nm, and in the case of exosomes from HIV-1 virus producing cells, they contain gag [51] and present spikes on their surface. The argument to be made is whether the sensitization effects observed are due to p24 release from contaminant exosomes rather than from viruses.

The first argument against the contamination of exosomes comes from infectivity data. While exosomes might contain gag and spikes, there was no literature found showing they are capable of causing infection. Since the trends observed with lysis and infectivity after cholesterol depletion correlate with each other, it is likely not due to exosomes. Secondly, gradient centrifugation, the method used to purify the pseudoviruses based on density, is believed to efficiently separate exosomes, which are less dense than viruses [98]. Markers for exosomes such as Acetycholinesterase, a GPCR based receptor found on exosomes [98] were not present in the viral cultures based on Ache activity. Finally, a consistent finding in the exosome field is the absence of the receptor CD45 on viruses and the presence of it on exosomes [51]. To test for the presence of CD45, pseudoviruses were run

in parallel to a pellet of HEK-293T cells on a 10% SDS-PAGE gel, transferred to a PVDF membrane and then detected using a rabbit anti-CD45 antibody (Abcam). The data showed CD45 in the cell pellet but not in the viruses.

In the next step, HEK-293T cells were co-transfected to produce BaL.01 pseudoviruses. The produced pseudoviruses were run through a gradient and every fraction collected was tested for infectivity, p24 content and the presence of CD45 using cell-based chemiluminescence, sandwich ELISA and western blot.

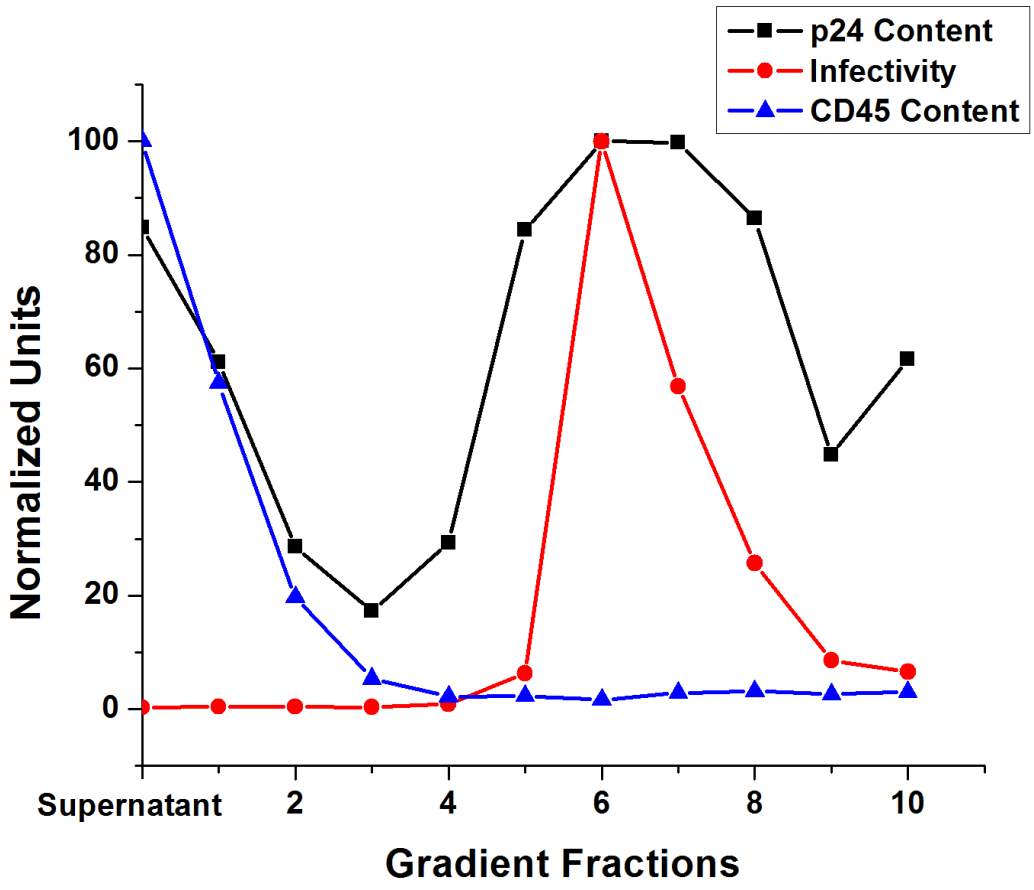

Figure 25: *Characterization of contents of Iodixanol gradient fractions used to purify BaL.01 pseudoviruses. Increasing numbers indicate increasing density. P24 content (black squares) was determined via sandwich ELISA while infectivty (red circles) was determined via cell based assay with chemiluminescence as an endpoint and CD45 content (blue triangles) was determined using Western Blot.*

The data in **Figure 25** suggest that CD45 was present in the supernatant collected from HEK-293T cells and in fractions (1, 2) that also have a lot of p24 content. However, it was not found in the fractions that were used to collect viruses from (6-9), based on infectivity values. These data suggest that the pseudoviruses used in this study are free of CD45-containing exosomes.

3. The final caveat to be considered is the impact of the level of spike gp120 in viruses on observed sensitization. MβCD treatments that result in shedding of gp120, reducing the number of active spikes on the envelope surface (**Figure 7**B) also result in enhancement of lysis (**Figure 5**B) and infectivity (**Figure 14**) though the shedding phenomena have not been linked with either. Protease treatments of the pseudovirus that are believed to result in fewer spikes that are "clean" and functional (50% drop) resulted in 200% enhancement in infectivity as shown in **Figure 26**.

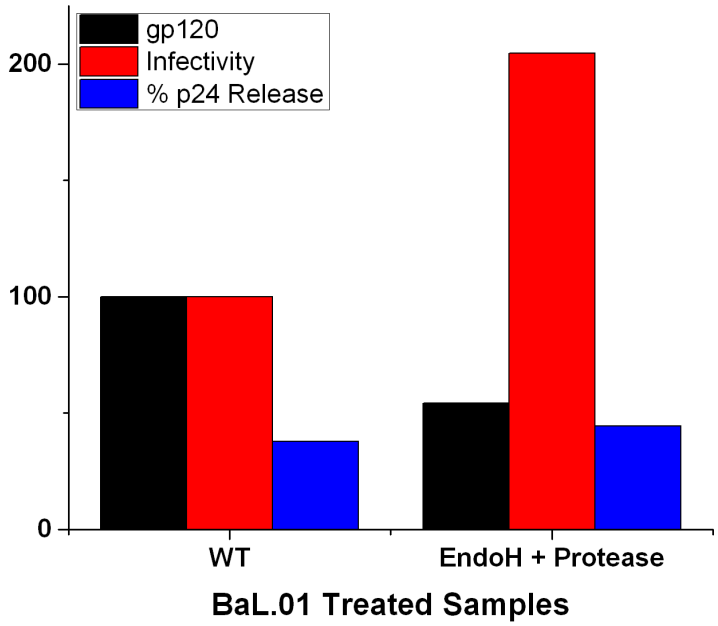

Figure 26: *Effect of protease purification on gp120 incorporation (black), infectivity (red) and lysis with 5 μM KR-13 (blue). BaL.01 pseudoviruses were treated with EndoH for 30 minutes followed by a cocktail containing trypsin, chymotrypsin and proteinase K for another 30 minutes. All treatments were done at 37C. Pseudovirus sample control was treated at the same temperature and time as the enzyme-treated sample except with PBS additions. Both samples were then run through an Iodixanol gradient and the resultant biochemical parameters measured by western blot (gp120), chemiluminescence (infectivity), and sandwich ELISA (lysis).*

In other work done in this thesis, pseudoviruses produced with different amount of spikes showed that while spike incorporation was proportional to the amount of spike DNA used in the co-transfection to produce pseudoviruses, infectivity was inversely proportional up to a low threshold below which it plateaued as shown in **Figure 27**.

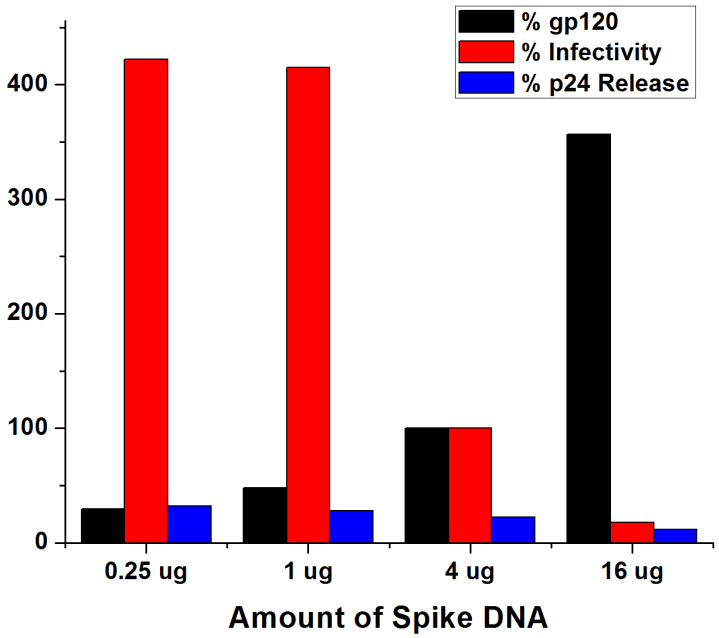

Figure 27: *Biochemical characterization of pseudoviruses made with different amounts of BaL.01 gp160 spike DNA. The pseudoviruses were characterized for gp120 content (western blots, black), infectivity (chemiluminescence, red) and lysis with 5 μM KR-13 (sandwich ELISA, red) and normalized for p24 content.*

Considering literature and the findings in this thesis, we could build an alternate model where reducing spike gp120 (before producing pseudoviruses by DNA amount reduction or after by protease treatments or MβCD treatments) results in

sensitization of the virus. Prior literature has shown that pseudoviruses produced with fewer spikes show enhanced infectivity and *vice versa* [99] consistent with the findings in this thesis.

The main finding that disagrees with this model is reversibility of lytic and infectivity trends with MβCD treatment with the supplementation of exogenous cholesterol. While the sterol can reverse lysis and infectivity, shedding of gp120 is believed to be irreversible [11]. Hence, the trends cannot be attributed to simple gp120 content incorporated on pseudovirions.

Consideration of these caveats is important to get a more balanced interpretation of the work presented in the previous chapters.

PUTATIVE MODELS THAT UNIFY THE DATA

The purpose of this section is to examine what is known about membranes and HIV-1 spikes in literature and determine, based on the data, a model to explain the findings. Three models will be developed for discussion.

Model # 1: Partial Depletion of Lipid Rafts Allows for Observed Enhancement of Lysis and Infectivity

The existence of lipid rafts on cell membranes has been proposed and mostly accepted since the findings that some proteins associate with detergent resistant membranes and float to the top of a density gradient in flotation assays. In these assays, it was determined that the proteins rose to the top with a mixture of certain lipids, namely cholesterol, sphingomyelin and GM1, a ganglioside which, along with mostly saturated phospholipids, result in rafts which are much more tightly packed compared to non-raft regions. Fluorescence microscopy coupled with advanced techniques such as Forster's Resonance Energy Transfer (FRET) have determined that these raft domains are between 10-100 nm in diameter. They are known to sequester certain proteins in the plasma membrane exclusively such as CD44, and to exclude others such as CD45.

HIV-1 budding is believed to occur in these raft domains resulting in high concentration of cholesterol (45 mol %) and SM (18 mol %). While it has not been determined, it is speculated that the viral envelope (membrane) is made up of rafts. As mentioned before, cholesterol depletion occurs preferentially in non-raft regions and this results in defined raft *vs.* non-raft regions. Flotation assays of gp41 in viral membranes revealed that it floats to the top suggesting it is raft-associated [19]. Other work has shown that the CRAC domain within gp41 prefers raft regions, and specifically the interface between raft and non-raft regions [100].

Other work has revealed that the interfaces between raft and non-raft regions contain a mismatch in lipid heights and make a weak region primed to be perturbed. Hence, if cholesterol depletion leads to increasing the length of these interfaces, it might provide access to more spikes to the interface allowing an enhancement of lysis (**Figure 5**B) and infectivity (**Figure 14**).

At higher depletion of cholesterol, infectivity gets arrested as does lysis with PTT. One possible explanation is the spike is no longer associated with rafts. This has been shown with flotation assays with gp41 no longer rising to the top after heavy cholesterol depletion (20,000 μM MβCD) though this association is re-established with supplementation of exogenous cholesterol [101].

The lipid raft model fits with the bell-shaped curve observed for lysis and infectivity with sensitizations at low treatments and abolishment at higher concentrations. It also fits with published replenishment data on infectivity especially with sterols that support rafts (cholesterol and cholestanol) vs. sterols that do not (coprostanol) [19]. However, for lysis, we observed that coprostanol led to intermediate recovery of lysis (instead of no recovery) while cholestanol led to complete recovery (**Figure 9**). The differences between cholestanol and coprostanol only became pronounced when larger amounts of cholesterol were depleted before exogenous supplementation (**Figure 10** and **Figure 11**). One explanation for this difference in coprostnol behavior might have to do with the presence

of rafts. If rafts are not completely destroyed (as we believe to be the case with more modest MβCD treatments), addition of alternate sterols simply reverses the effect of removing cholesterol, namely adding bulk to the membrane. This might not require a particular type of sterol. However, when the raft is more completely destroyed, as could occur at high treatments of MβCD, the type of sterol added might determine if a raft re-forms or not. The concept of large-scale disruption is supported by the changing fluidity data at higher amounts of MβCD treatment.

Model # 2: Clustering of Spikes Results in Enhancement of Lysis and Infectivity

Fully infectious virions are believed to have between 8-14 spikes [67] while pseudoviruses can have more depending on the ratio of spike DNA to core DNA used in co-transfections (**Figure 27**). Originally, the spikes were believed to be evenly spread, throughout the surface until the first super-resolution images challenged the view [102]. The images suggested that spikes on mature viral particles tended to cluster in groups on virion and this ability to cluster was lost in immature particles (uncleaved gag) or in virions where the spike was missing the C-terminal tail resulting in no or reduced infectivity respectively. Other groups found that each virus type has a certain minimum number of spikes required for infection and, the more spikes expressed than what is needed, the greater the observed infectivity, possibly due to the higher chance of interaction between a spike and cellular receptors [67]. These findings, combined with early cryo-TEM micrographs of the

virological synapse filled with spikes [103, 104], suggest that the clustering of spikes is beneficial for infectivity.

This model on clustering fits well with the idea of what happens as cholesterol is depleted from the viral envelope. The raft regions would shrink and the spikes which have an affinity for the raft regions would cluster so as to remain on the raft, thereby making it more likely for a positive interaction to occur when the virion interacted with a cell expressing CD4 and co-receptor. This enhancement/greater likelihood of a productive encounter would remain while the raft was not completely depleted. Once the threshold is crossed, the spikes would possibly spread out, with nothing keeping them together. This idea would fit well with the bell-shaped infectivity trend but there is no evidence linking this model with lysis.

In investigations on proximity requirements, it was determined by using mutants expressing different ratios of S375W (a mutation in gp120 that retains infectivity but suppreses the binding of peptide triazole thiols [105]) to WT gp120, that proximity between units of WT gp120 was not critical for lysis [106] as long as there was at least one complete trimeric spike made up of three WT gp120 units.

The other control used to judge the validity model is the work done with the CRAC and C-tail truncation (R706St) mutant pseudoviruses as well as the double mutant. Since the CRAC region is important in recruiting spikes to raft regions [100], mutating it out using a Leu -> Ile mutation should stop recruitment to raft regions. Similarly, The C-tail truncation mutant has been shown not to cluster in the native state ([102]). Hence, if clustering is important for enhancement in infectivity and lysis, neither mutant should show

enhancement with progressive cholesterol depletion. However, this is not true as observed in **Figure 20**. The CRAC mutant and the double mutant (CRAC + R706St) show bell-shaped curves albeit with diminished overall sensitivity. Hence, based on the available data, this model is not accepted.

Model # 3: Formation of gp41 6-Helix Bundle Determines the Observed Enhancement in Lysis and Fusion

After the interaction of gp120 with CD4, the most energy-releasing reaction is the formation of the 6-helix bundle based on calorimetric analysis with peptide mimics. The energy released in the formation of the 6-HB is believed to be used in the fusion of the membranes [45], though how this occurs has not been determined. One possibility is the formation of the 6-helix bundle is tied to a second process that requires a lot of energy and the two processes are in equilibrium with the event of CD4/co-receptor binding tipping the equilibrium toward 6-HB formation. This could be due to (1) Spatial requirements since a large segment of the gp41 protein (3x NHR + CHR) comes in close proximity, possibly perturbing the membrane during hydrophobic collapse. (2) Bending of the membrane that might happen between the three gp41 units connected to the membrane during the 6-HB formation. Or (3) Exposure of the MPER domains during fusion. MPER is known to become exposed post-CD4 and co-receptor binding [107-109] and this transition of MPER might be energy intensive.

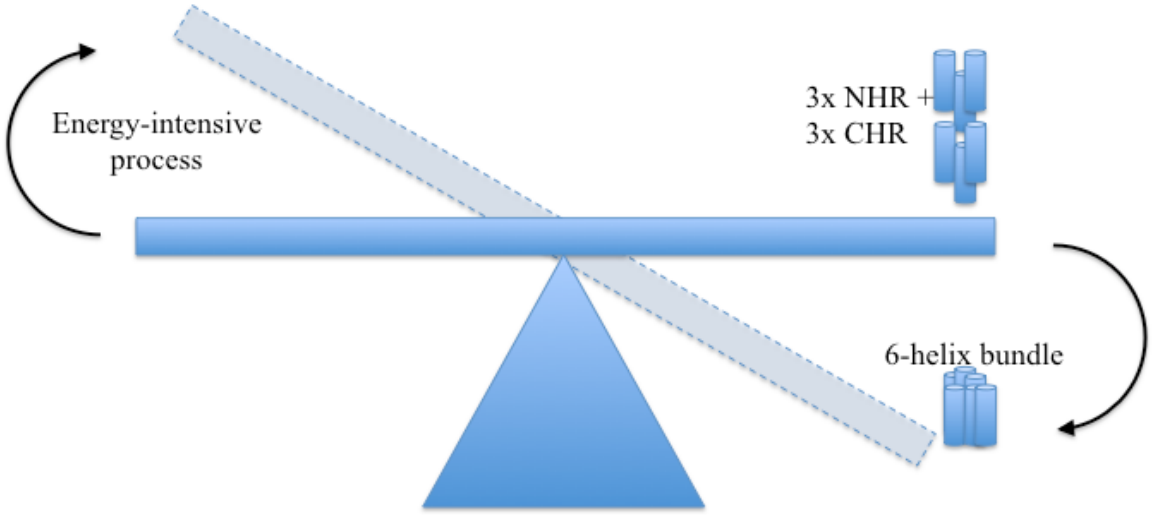

Figure 28: *Illustration of the equilibrium that must be perturbed to form the 6-helix bundle*

Regardless of how the energy released from 6-HB formation is used, if the system in equilibrium is changed to reduce the energy-intensive process through a process such as depleting cholesterol, it would drive the system into forming 6-helix bundles with more likelihood. One reason for the depletion to have this effect is that when more than 60% of cholesterol is depleted at the maximum enhancement in lysis and infectivity (**Figure 7**A), there might be more space within the bilayer which may make it easier spatially for bundles to form and easier to bend membranes if that were the determinant. Another reason may have to do with the CRAC domain in MPER interacting with cholesterol. With majority of the cholesterol depleted, it might have a lower number of interactions with the surrounding membrane, which might make MPER transitions easier to occur resulting in the observed enhancement with infectivity and lysis. However, this model should be linear

with cholesterol depletion and does not fit the bell-shaped trend observed with lysis and infectivity at greater MβCD treatments making it difficult to pick this model.

Conclusions:

Based on the three models investigated, the lipid raft model fits with more findings than the other models. However, the other two models cannot be completely excluded based on the data. The clustering model, while it supported the observations with infectivity, did not have any data to support observations with lysis. The 6-helix bundle requirement model, while it supported the enhancement findings for lysis and infectivity, did not explain why we see a drop at higher cholesterol depletion.

It seems no model completely explains all the findings but each model supports certain aspects. Some of the findings are quite new such as clustering of spikes and more investigations are required to determine the mechanism. Others are poorly understood such as how 6-helix bundle formation directly translates to membrane perturbation and fusion. Based on what is known now, we must accept that further findings on these models are required to shed light on the complete mechanism by which cholesterol depletion results in bell-shaped trends in lysis with PTT and infectivity.

FUTURE DIRECTIONS:

When investigating cholesterol and the ability of different sterols to recover lysis, cholestanol and coprostanol were tested since the former is known to support rafts and the latter does not [19]. The data obtained were interesting. However, a main weakness was the lack of proof that the added sterols inserted into the lipid bilayer. This could be remedied by visualizing the change in buoyant densities by running the treated virus samples and controls on Iodixanol gradients and visualizing the recovery of the density with the addition of the sterol after MβCD treatment. The findings between cholestanol and coprostanol can be strengthened by testing other sterols such as Dihydrocholesterol, 7-dehydrocholesterol, epicholesterol which support rafts and 4-cholestenone which does not [19].

The membrane morphology data acquired with Dehydroergosterol and the lytic recovery data with different sterols suggested that rafts might play a role in spike activity. A recent paper has provided evidence that the N-terminal fusion peptide on gp41 actively seeks out the interface between raft and non-raft domains on the cell membrane to insert into to start fusion [110]. It is not too far a stretch that a similar interface on the viral envelope could help kick things along. At ~45 mol % cholesterol, the envelope is believed to be in a gel phase but small amounts of depletion might result in a membrane with distinct raft and non-raft regions. While they cannot be visualized without super-resolution microscopy, they are in the ball park of FRET measurements (1 nm < r_o < 10 nm) with a pair of

membrane-embedded fluorophores such as Dehydroergosterol, a fluorescent sterol that closely mimics the raft preference of cholesterol [111] and an acyl chain-bound partner such as Dansyl or NBD. By modifying the amount of the acceptor within the assays, it will be possible to calculate the size of the raft domains with changing amounts of the depletion agent. This could foster new understanding of the location and behavior of the spike.

Treatment of pseudoviruses with PTTs has shown an enhanced exposure of the conserved MPER epitope based on binding data with MPER antibodies 2F5, 4E10 and 10E8 leading residual virions to be attractive vaccine candidates in mouse studies [11]. Pre-treatment of the same pseudoviruses with low amounts of MβCD before the addition of PTT significantly enhances the lytic release of capsid p24 protein. Removing sterol from the viral membrane is known to affect the location of the CRAC domain along the normal to the viral envelope [38] and might make it easier for antibody access. Hence, it would be worthwhile to test if treatment with MβCD alone or pre-treatment with MβCD followed by KR-13 would significantly enhance the conserved MPER epitope exposure resulting in a better immunogen for vaccine studies.

Investigations with the protein mutants that targeted the ability of gp41 to interact with the viral envelop led to some tantalizing findings. The CRAC mutant and the C-terminal tail truncation mutant showed enhancement with lower amounts of MβCD than wild type or other mutants. It would be worthwhile confirming cholesterol content and shedding of

gp120 to understand the behavior observed with these mutants. Does cholesterol content change with smaller amounts of MβCD treatment for the mutants as compared to the wild-type virus? If we assumed that viral gp120 shedding occurred as a function of cholesterol removal, would this enhance shedding observed at lower amounts of MβCD?

This finding can be verified with other mutants that have intermediate levels of CRAC activity such as LWGIG or GWGIK. It would be worthwhile knowing if they also exhibited enhancement at doses of MβCD less than the ones shown for wild-type as this would establish a pattern of behavior for the CRAC region. The C-terminal tail also has two putative CRAC domains which are removed in the truncation mutation. It would be worthwhile creating a new mutant that moves the stop codon down toward the C-terminus allowing the expression of one or both regions and investigating if this alleviates the early sensitization observed. Getting these data would allow us to make stronger observations of the behavior of these regions.

A major argument for the enhancement effects presented in chapter 2 and chapter 3 is a lowering of the energy barrier a spike would have to cross in order to initiate fusion (or lysis) by extracting spike cholesterol. A recent publication demonstrated that viruses of different clades have different levels of infectivity based on the number of spikes they might need to recruit in order to carry out fusion [67]. While there is thermodynamic and mathematical proof that a single spike undergoing 6-helix bundle formation releases enough energy for fusion [45], a review of literature suggests this number is between 2 and

8 depending on the virus isolate chosen [67]. This publication showed that viruses with lower infectivity (possibly due to more inefficient bundle formation) recruited more spikes for fusion, which in turn meant a slower process compared to isolates that required fewer spikes. If the energy barrier is being lowered by cholesterol extraction, the number of spikes required to carry out fusion/lysis might be reduced or at the very least, speeded up compared to an untreated virus sample. This can be tested with the timed addition of inhibitors to lysis and fusion such as T-20 or C-37 or 5-helix which bind to and inhibit the formation of the 6-helix bundle.

Alternatively, the publication sought the use of mixtures of different ratios of dominant negative mutants (cleavage deficient where gp120 and gp41 remain a single unit and fusion mutant, V2E, which has been tested in chapter 3) in combination with wild-type spikes on the same pseudovirus to demonstrate the change in number of spikes required to carry out fusion. While the V2E mutant will not suppress lysis as we found in chapter 3, the cleavage deficient mutant might prove to be useful in determining whether the number of spikes required for infection and lysis drops after small amounts of MβCD treatment.

Bibliography

1. Harrison, S.C., *Viral membrane fusion.* Nat Struct Mol Biol, 2008. **15**(7): p. 690-8.

2. Lederman, M.M., et al., *Topical application of entry inhibitors as "virustats" to prevent sexual transmission of HIV infection.* Retrovirology, 2008. **5**: p. 116.

3. Sundquist, W.I. and H.G. Krausslich, *HIV-1 assembly, budding, and maturation.* Cold Spring Harb Perspect Med, 2012. **2**(7): p. a006924.

4. Aiken, C. and P. Zhang, *HIV-1 Maturation*, in *Advances in HIV-1 Assembly and Release*, E.O. Freed, Editor. 2013, Springer New York. p. 153-166.

5. Coutinho, B. and R. Prasad, *Emtricitabine/tenofovir (Truvada) for HIV prophylaxis.* Am Fam Physician, 2013. **88**(8): p. 535-40.

6. Breeze, S., *FDA PrEPares to reduce risk of HIV infection with Truvada(R).* Expert Rev Clin Pharmacol, 2012. **5**(5): p. 499.

7. Kuritzkes, D.R., *HIV-1 entry inhibitors: an overview.* Curr Opin HIV AIDS, 2009. **4**(2): p. 82-7.

8. Gopi, H., et al., *Introducing metallocene into a triazole peptide conjugate reduces its off-rate and enhances its affinity and antiviral potency for HIV-1 gp120.* J Mol Recognit, 2009. **22**(2): p. 169-74.

9. Umashankara, M., et al., *The active core in a triazole peptide dual-site antagonist of HIV-1 gp120.* ChemMedChem, 2010. **5**(11): p. 1871-9.

10. McFadden, K., et al., *Antiviral breadth and combination potential of peptide triazole HIV-1 entry inhibitors.* Antimicrob Agents Chemother, 2012. **56**(2): p. 1073-80.

11. Bastian, A.R., et al., *Interactions of peptide triazole thiols with Env gp120 induce irreversible breakdown and inactivation of HIV-1 virions.* Retrovirology, 2013. **10**: p. 153.

12. Brugger, B., et al., *The HIV lipidome: a raft with an unusual composition.* Proceedings of the National Academy of Sciences of the United States of America, 2006. **103**(8): p. 2641-6.

13. Chan, D.C., et al., *Core structure of gp41 from the HIV envelope glycoprotein.* Cell, 1997. **89**(2): p. 263-73.

14. Lorizate, M., et al., *Comparative lipidomics analysis of HIV-1 particles and their producer cell membrane in different cell lines.* Cell Microbiol, 2013. **15**(2): p. 292-304.

15. Sun, X. and G.R. Whittaker, *Role for influenza virus envelope cholesterol in virus entry and infection.* J Virol, 2003. **77**(23): p. 12543-51.

16. Scheiffele, P., M.G. Roth, and K. Simons, *Interaction of influenza virus haemagglutinin with sphingolipid-cholesterol membrane domains via its transmembrane domain.* EMBO J, 1997. **16**(18): p. 5501-8.

17. Bavari, S., et al., *Lipid raft microdomains: a gateway for compartmentalized trafficking of Ebola and Marburg viruses.* J Exp Med, 2002. **195**(5): p. 593-602.

18. Carro, A.C. and E.B. Damonte, *Requirement of cholesterol in the viral envelope for dengue virus infection.* Virus Res, 2013. **174**(1-2): p. 78-87.

19. Campbell, S., et al., *The raft-promoting property of virion-associated cholesterol, but not the presence of virion-associated Brij 98 rafts, is a determinant of human immunodeficiency virus type 1 infectivity.* Journal of Virology, 2004. **78**(19): p. 10556-65.

20. Campbell, S.M., S.M. Crowe, and J. Mak, *Lipid rafts and HIV-1: from viral entry to assembly of progeny virions.* J Clin Virol, 2001. **22**(3): p. 217-27.

21. Graham, D.R., et al., *Cholesterol depletion of human immunodeficiency virus type 1 and simian immunodeficiency virus with beta-cyclodextrin inactivates and permeabilizes the virions: evidence for virion-associated lipid rafts.* Journal of Virology, 2003. **77**(15): p. 8237-48.

22. Liao, Z., et al., *Lipid rafts and HIV pathogenesis: host membrane cholesterol is required for infection by HIV type 1.* AIDS Res Hum Retroviruses, 2001. **17**(11): p. 1009-19.

23. Liao, Z., D.R. Graham, and J.E. Hildreth, *Lipid rafts and HIV pathogenesis: virion-associated cholesterol is required for fusion and infection of susceptible cells.* AIDS Res Hum Retroviruses, 2003. **19**(8): p. 675-87.

24. Nguyen, D.H. and D. Taub, *CXCR4 function requires membrane cholesterol: implications for HIV infection.* J Immunol, 2002. **168**(8): p. 4121-6.

25. Ivankin, A., I. Kuzmenko, and D. Gidalevitz, *Cholesterol mediates membrane curvature during fusion events.* Phys Rev Lett, 2012. **108**(23): p. 238103.

26. Ramstedt, B. and J.P. Slotte, *Interaction of cholesterol with sphingomyelins and acyl-chain-matched phosphatidylcholines: a comparative study of the effect of the chain length.* Biophys J, 1999. **76**(2): p. 908-15.

27. Coren, L.V., T. Shatzer, and D.E. Ott, *CD45 immunoaffinity depletion of vesicles from Jurkat T cells demonstrates that exosomes contain CD45: no evidence for a distinct exosome/HIV-1 budding pathway.* Retrovirology, 2008. **5**: p. 64.

28. Park, I.W. and J.J. He, *HIV-1 is budded from CD4+ T lymphocytes independently of exosomes.* Virol J, 2010. **7**: p. 234.

29. Esser, M.T., et al., *Differential incorporation of CD45, CD80 (B7-1), CD86 (B7-2), and major histocompatibility complex class I and II molecules into human immunodeficiency virus type 1 virions and microvesicles: implications for viral pathogenesis and immune regulation.* J Virol, 2001. **75**(13): p. 6173-82.

30. Ono, A. and E.O. Freed, *Plasma membrane rafts play a critical role in HIV-1 assembly and release.* Proc Natl Acad Sci U S A, 2001. **98**(24): p. 13925-30.

31. Briggs, J.A.G., T. Wilk, and S.D. Fuller, *Do llpid rafts mediate virus assembly and pseudotyping?* Journal of General Virology, 2003. **84**: p. 757-768.

32. Munoz-Barroso, I., et al., *Role of the membrane-proximal domain in the initial stages of human immunodeficiency virus type 1 envelope glycoprotein-mediated membrane fusion.* J Virol, 1999. **73**(7): p. 6089-92.

33. Salzwedel, K., J.T. West, and E. Hunter, *A conserved tryptophan-rich motif in the membrane-proximal region of the human immunodeficiency virus type 1 gp41 ectodomain is important for Env-mediated fusion and virus infectivity.* J Virol, 1999. **73**(3): p. 2469-80.

34. Song, L., et al., *Broadly neutralizing anti-HIV-1 antibodies disrupt a hinge-related function of gp41 at the membrane interface.* Proc Natl Acad Sci U S A, 2009. **106**(22): p. 9057-62.

35. Epand, R.F., B.G. Sayer, and R.M. Epand, *The tryptophan-rich region of HIV gp41 and the promotion of cholesterol-rich domains.* Biochemistry, 2005. **44**(14): p. 5525-31.

36. Epand, R.F., et al., *Juxtamembrane protein segments that contribute to recruitment of cholesterol into domains.* Biochemistry, 2006. **45**(19): p. 6105-14.

37. Vishwanathan, S.A., et al., *Large changes in the CRAC segment of gp41 of HIV do not destroy fusion activity if the segment interacts with cholesterol.* Biochemistry, 2008. **47**(45): p. 11869-76.

38. Vishwanathan, S.A., et al., *Hydrophobic substitutions in the first residue of the CRAC segment of the gp41 protein of HIV.* Biochemistry, 2008. **47**(1): p. 124-30.

39. Gangupomu, V.K. and C.F. Abrams, *All-atom models of the membrane-spanning domain of HIV-1 gp41 from metadynamics.* Biophys J, 2010. **99**(10): p. 3438-44.

40. Vostrikov, V.V., et al., *Accommodation of a central arginine in a transmembrane peptide by changing the placement of anchor residues.* J Phys Chem B, 2012. **116**(43): p. 12980-90.

41. Long, Y., et al., *Conserved arginine residue in the membrane-spanning domain of HIV-1 gp41 is required for efficient membrane fusion.* Protein Cell, 2011. **2**(5): p. 369-76.

42. Costin, J.M., et al., *Viroporin potential of the lentivirus lytic peptide (LLP) domains of the HIV-1 gp41 protein.* Virol J, 2007. **4**: p. 123.

43. Waheed, A.A., et al., *HIV-1 escape from the entry-inhibiting effects of a cholesterol-binding compound via cleavage of gp41 by the viral protease.* Proc Natl Acad Sci U S A, 2007. **104**(20): p. 8467-71.

44. Helseth, E., et al., *Rapid complementation assays measuring replicative potential of human immunodeficiency virus type 1 envelope glycoprotein mutants.* Journal of virology, 1990. **64**(5): p. 2416-20.

45. Blumenthal, R., S. Durell, and M. Viard, *HIV entry and envelope glycoprotein-mediated fusion.* J Biol Chem, 2012. **287**(49): p. 40841-9.

46. Bastian, A.R., et al., *Cell-free HIV-1 virucidal action by modified peptide triazole inhibitors of Env gp120.* ChemMedChem, 2011. **6**(8): p. 1335-9, 1318.

47. Chan, R., et al., *Retroviruses human immunodeficiency virus and murine leukemia virus are enriched in phosphoinositides.* J Virol, 2008. **82**(22): p. 11228-38.

48. Domanska, M.K., D. Wrona, and P.M. Kasson, *Multiphasic effects of cholesterol on influenza fusion kinetics reflect multiple mechanistic roles.* Biophys J, 2013. **105**(6): p. 1383-7.

49. Bailey, L.D., Li, H., Kalyana Sundaram, R. V., Duffy, C., Aneja, R., Rosemary Bastian, A., Holmes, A. P., Kamanna, K., Rashad, A. A. and Chaiken, I., *Spatial Relationship between the Binding Pharmacophore and Sulfhydryl Structural Motifs of Peptide Triazole Thiols that Enables HIV-1 Lytic Inactivation.* Journal of Medicinal Chemistry, 2014 (submitted).

50. Montefiori, D.C., *Evaluating Neutralizing Antibodies Against HIV, SIV, and SHIV in Luciferase Reporter Gene Assays.* Current Protocols in Immunology, 2005. **64**: p. 12.11.1-12.11.17.

51. Booth, A.M., et al., *Exosomes and HIV Gag bud from endosome-like domains of the T cell plasma membrane.* J Cell Biol, 2006. **172**(6): p. 923-35.

52. Crooks, E.T., et al., *Enzyme digests eliminate nonfunctional Env from HIV-1 particle surfaces, leaving native Env trimers intact and viral infectivity unaffected.* J Virol, 2011. **85**(12): p. 5825-39.

53. Lorizate, M., et al., *Probing HIV-1 Membrane Liquid Order by Laurdan Staining Reveals Producer Cell-dependent Differences.* Journal of Biological Chemistry, 2009. **284**(33): p. 22238-22247.

54. McIntosh, A.L., et al., *Fluorescence techniques using dehydroergosterol to study cholesterol trafficking.* Lipids, 2008. **43**(12): p. 1185-208.

55. Chong, P.L., *Evidence for regular distribution of sterols in liquid crystalline phosphatidylcholine bilayers.* Proc Natl Acad Sci U S A, 1994. **91**(21): p. 10069-73.

56. Mukherjee, S., et al., *Cholesterol distribution in living cells: Fluorescence imaging using dehydroergosterol as a fluorescent cholesterol analog.* Biophysical Journal, 1998. **75**(4): p. 1915-1925.

57. Wustner, D., et al., *Rapid nonvesicular transport of sterol between the plasma membrane domains of polarized hepatic cells.* Journal of Biological Chemistry, 2002. **277**(33): p. 30325-30336.

58. Thorp, E.B. and T.M. Gallagher, *Requirements for CEACAMs and cholesterol during murine coronavirus cell entry.* J Virol, 2004. **78**(6): p. 2682-92.

59. Bourguignon, L.Y., et al., *CD44 interaction with Na+-H+ exchanger (NHE1) creates acidic microenvironments leading to hyaluronidase-2 and cathepsin B activation and breast tumor cell invasion.* J Biol Chem, 2004. **279**(26): p. 26991-7007.

60. Eskelinen, E.L., et al., *Disturbed cholesterol traffic but normal proteolytic function in LAMP-1/LAMP-2 double-deficient fibroblasts.* Mol Biol Cell, 2004. **15**(7): p. 3132-45.

61. Nilsson, A., *The presence of spingomyelin- and ceramide-cleaving enzymes in the small intestinal tract.* Biochim Biophys Acta, 1969. **176**(2): p. 339-47.

62. Lopez, C.A., A.H. de Vries, and S.J. Marrink, *Computational microscopy of cyclodextrin mediated cholesterol extraction from lipid model membranes.* Scientific Reports, 2013. **3**.

63. Tong, T., et al., *HIV-1 virus-like particles bearing pure env trimers expose neutralizing epitopes but occlude nonneutralizing epitopes.* J Virol, 2012. **86**(7): p. 3574-87.

64. Aloia, R.C., et al., *Lipid composition and fluidity of the human immunodeficiency virus.* Proceedings of the National Academy of Sciences of the United States of America, 1988. **85**(3): p. 900-4.

65. Aloia, R.C., H. Tian, and F.C. Jensen, *Lipid composition and fluidity of the human immunodeficiency virus envelope and host cell plasma membranes.* Proceedings of the National Academy of Sciences of the United States of America, 1993. **90**(11): p. 5181-5.

66. Smutzer, G., B.F. Crawford, and P.L. Yeagle, *Physical properties of the fluorescent sterol probe dehydroergosterol.* Biochim Biophys Acta, 1986. **862**(2): p. 361-71.

67. Brandenberg, O.F., et al., *Different infectivity of HIV-1 strains is linked to number of envelope trimers required for entry.* PLoS Pathog, 2015. **11**(1): p. e1004595.

68. Nguyen, D.H. and D. Taub, *Cholesterol is essential for macrophage inflammatory protein 1 beta binding and conformational integrity of CC chemokine receptor 5.* Blood, 2002. **99**(12): p. 4298-306.

69. Pontier, S.M., et al., *Cholesterol-dependent separation of the beta2-adrenergic receptor from its partners determines signaling efficacy: insight into nanoscale organization of signal transduction.* J Biol Chem, 2008. **283**(36): p. 24659-72.

70. Pucadyil, T.J. and A. Chattopadhyay, *Cholesterol modulates ligand binding and G-protein coupling to serotonin(1A) receptors from bovine hippocampus.* Biochim Biophys Acta, 2004. **1663**(1-2): p. 188-200.

71. Klein, U., G. Gimpl, and F. Fahrenholz, *Alteration of the myometrial plasma membrane cholesterol content with beta-cyclodextrin modulates the binding affinity of the oxytocin receptor.* Biochemistry, 1995. **34**(42): p. 13784-93.

72. Lyumkis, D., et al., *Cryo-EM structure of a fully glycosylated soluble cleaved HIV-1 envelope trimer.* Science, 2013. **342**(6165): p. 1484-90.

73. Julien, J.P., et al., *Crystal structure of a soluble cleaved HIV-1 envelope trimer.* Science, 2013. **342**(6165): p. 1477-83.

74. Kassa, A., et al., *Transitions to and from the CD4-bound conformation are modulated by a single-residue change in the human immunodeficiency virus type 1 gp120 inner domain.* J Virol, 2009. **83**(17): p. 8364-78.

75. Kassa, A., et al., *Identification of a human immunodeficiency virus type 1 envelope glycoprotein variant resistant to cold inactivation.* J Virol, 2009. **83**(9): p. 4476-88.

76. Epand, R.M., *Cholesterol and the interaction of proteins with membrane domains.* Prog Lipid Res, 2006. **45**(4): p. 279-94.

77. Epand, R.M., *Proteins and cholesterol-rich domains.* Biochim Biophys Acta, 2008. **1778**(7-8): p. 1576-82.

78. Zocher, M., et al., *Cholesterol increases kinetic, energetic, and mechanical stability of the human beta2-adrenergic receptor.* Proc Natl Acad Sci U S A, 2012. **109**(50): p. E3463-72.

79. Hanson, M.A., et al., *A specific cholesterol binding site is established by the 2.8 A structure of the human beta2-adrenergic receptor.* Structure, 2008. **16**(6): p. 897-905.

80. Needham, D. and R.S. Nunn, *Elastic deformation and failure of lipid bilayer membranes containing cholesterol.* Biophys J, 1990. **58**(4): p. 997-1009.

81. van Meer, G. and A.I. de Kroon, *Lipid map of the mammalian cell.* J Cell Sci, 2011. **124**(Pt 1): p. 5-8.

82. van Meer, G., D.R. Voelker, and G.W. Feigenson, *Membrane lipids: where they are and how they behave.* Nat Rev Mol Cell Biol, 2008. **9**(2): p. 112-24.

83. Lopez, C.A., A.H. de Vries, and S.J. Marrink, *Computational microscopy of cyclodextrin mediated cholesterol extraction from lipid model membranes.* Sci Rep, 2013. **3**: p. 2071.

84. Yancey, P.G., et al., *Cellular cholesterol efflux mediated by cyclodextrins. Demonstration Of kinetic pools and mechanism of efflux.* J Biol Chem, 1996. **271**(27): p. 16026-34.

85. Vishwanathan, S.A. and E. Hunter, *Importance of the membrane-perturbing properties of the membrane-proximal external region of human immunodeficiency virus type 1 gp41 to viral fusion.* J Virol, 2008. **82**(11): p. 5118-26.

86. Zwick, M.B., *The membrane-proximal external region of HIV-1 gp41: a vaccine target worth exploring.* AIDS, 2005. **19**(16): p. 1725-37.

87. Vanlandschoot, P., et al., *An antibody which binds to the membrane-proximal end of influenza virus haemagglutinin (H3 subtype) inhibits the low-pH-induced conformational change and cell-cell fusion but does not neutralize virus.* J Gen Virol, 1998. **79 (Pt 7)**: p. 1781-91.

88. Weissenhorn, W., et al., *The central structural feature of the membrane fusion protein subunit from the Ebola virus glycoprotein is a long triple-stranded coiled coil.* Proc Natl Acad Sci U S A, 1998. **95**(11): p. 6032-6.

89. Sanchez, S.A., et al., *Methyl-beta-cyclodextrins preferentially remove cholesterol from the liquid disordered phase in giant unilamellar vesicles.* J Membr Biol, 2011. **241**(1): p. 1-10.

90. Ohtani, Y., et al., *Differential effects of alpha-, beta- and gamma-cyclodextrins on human erythrocytes.* Eur J Biochem, 1989. **186**(1-2): p. 17-22.

91. Kilsdonk, E.P., et al., *Cellular cholesterol efflux mediated by cyclodextrins.* J Biol Chem, 1995. **270**(29): p. 17250-6.

92. Rog, T. and M. Pasenkiewicz-Gierula, *Cholesterol-sphingomyelin interactions: a molecular dynamics simulation study.* Biophys J, 2006. **91**(10): p. 3756-67.

93. Tsamaloukas, A., H. Szadkowska, and H. Heerklotz, *Thermodynamic comparison of the interactions of cholesterol with unsaturated phospholipid and sphingomyelins.* Biophys J, 2006. **90**(12): p. 4479-87.

94. Amundson, D.M. and M. Zhou, *Fluorometric method for the enzymatic determination of cholesterol.* J Biochem Biophys Methods, 1999. **38**(1): p. 43-52.

95. Xu, X. and E. London, *The effect of sterol structure on membrane lipid domains reveals how cholesterol can induce lipid domain formation.* Biochemistry, 2000. **39**(5): p. 843-9.

96. Hao, S., T. Moyana, and J. Xiang, *Review: cancer immunotherapy by exosome-based vaccines.* Cancer Biother Radiopharm, 2007. **22**(5): p. 692-703.

97. Stoorvogel, W., et al., *The biogenesis and functions of exosomes.* Traffic, 2002. **3**(5): p. 321-30.

98. Cantin, R., et al., *Discrimination between exosomes and HIV-1: purification of both vesicles from cell-free supernatants.* J Immunol Methods, 2008. **338**(1-2): p. 21-30.

99. Bachrach, E., et al., *Effects of virion surface gp120 density on infection by HIV-1 and viral production by infected cells.* Virology, 2005. **332**(1): p. 418-29.

100. Schwarzer, R., et al., *The cholesterol-binding motif of the HIV-1 glycoprotein gp41 regulates lateral sorting and oligomerization.* Cell Microbiol, 2014.

101. Yang, P., et al., *The cytoplasmic domain of human immunodeficiency virus type 1 transmembrane protein gp41 harbors lipid raft association determinants.* J Virol, 2010. **84**(1): p. 59-75.

102. Chojnacki, J. and B. Muller, *Investigation of HIV-1 assembly and release using modern fluorescence imaging techniques.* Traffic, 2013. **14**(1): p. 15-24.

103. Subramaniam, S., et al., *Electron tomography of viruses.* Curr Opin Struct Biol, 2007. **17**(5): p. 596-602.

104. Sougrat, R., et al., *Electron tomography of the contact between T cells and SIV/HIV-1: implications for viral entry.* PLoS Pathog, 2007. **3**(5): p. e63.

105. Biorn, A.C., et al., *Mode of action for linear peptide inhibitors of HIV-1 gp120 interactions.* Biochemistry, 2004. **43**(7): p. 1928-38.

106. Rosemary Bastian, A., et al., *Mechanism of multivalent nanoparticle encounter with HIV-1 for potency enhancement of peptide triazole virus inactivation.* J Biol Chem, 2015. **290**(1): p. 529-43.

107. Dimitrov, A.S., et al., *Exposure of the membrane-proximal external region of HIV-1 gp41 in the course of HIV-1 envelope glycoprotein-mediated fusion.* Biochemistry, 2007. **46**(5): p. 1398-401.

108. Rathinakumar, R., et al., *Binding of anti-membrane-proximal gp41 monoclonal antibodies to CD4-liganded and -unliganded human immunodeficiency virus type 1 and simian immunodeficiency virus virions.* J Virol, 2012. **86**(3): p. 1820-31.

109. Peachman, K.K., et al., *The effect of sCD4 on the binding and accessibility of HIV-1 gp41 MPER epitopes to human monoclonal antibodies.* Virology, 2010. **408**(2): p. 213-23.

110. Yang, S.T., et al., *HIV gp41-mediated membrane fusion occurs at edges of cholesterol-rich lipid domains.* Nat Chem Biol, 2015. **11**(6): p. 424-431.

111. Mukherjee, S., et al., *Cholesterol distribution in living cells: fluorescence imaging using dehydroergosterol as a fluorescent cholesterol analog.* Biophys J, 1998. **75**(4): p. 1915-25.